UNIVERSIDADE FEDERAL DE MINAS GERAIS
Instituto de Geociências
Programa de Pós-Graduação em Geologia

João Pedro Torrezani Martins Hippertt

THE FATE OF A NEOPROTEROZOIC INTRACRATONIC MARINE BASIN: TRACE ELEMENTS, TOC AND IRON SPECIATION GEOCHEMISTRY OF THE BAMBUÍ BASIN, BRAZIL

Nº186

BELO HORIZONTE
DATA (28/06/2018)

João Pedro Torrezani Martins Hippertt

THE FATE OF A NEOPROTEROZOIC INTRACRATONIC MARINE BASIN: TRACE ELEMENTS, TOC AND IRON SPECIATION GEOCHEMISTRY OF THE BAMBUÍ BASIN, BRAZIL

Dissertação de Mestrado

Dissertação apresentada ao Programa de Pós-Graduação em Geologia da Universidade Federal de Minas Gerais como requisito parcial para obtenção do título de mestre em Geologia.

Área de Concentração: Evolução Crustal e Recursos Minerais

Orientador(a): Prof. Dr. Fabrício de Andrade Caxito

Belo Horizonte
2018

H667f Hippertt, João Pedro Torrezani Martins.
2018 The fate of a neoproterozoic intracratonic marine basin [manuscrito] : trace elements, TOC and iron speciation geochemistry of The Bambuí Basin, Brazil / João Pedro Torrezani Martins Hippertt – 2018.
63 f., enc. (principalmente color.)

Orientador: Fabrício de Andrade Caxito.

Dissertação (mestrado) – Universidade Federal de Minas Gerais, Instituto de Geociências, 2018.

Área de concentração: Geologia Econômica e Aplicada.

Bibliografia: f. 49-62.

Inclui anexos.

1. Geoquímica – Teses. 2. Tempo geológico – Teses. 3. Mapeamento geológico – Teses. 4. São Francisco, Rio, Bacia – Teses. I. Caxito, Fabrício de Andrade. II. Universidade Federal de Minas Gerais. Instituto de Geociências. III. Título.

CDU: 550.4

Ficha catalográfica elaborada por Graciane A. de Paula – CRB6 3404

FOLHA DE APROVAÇÃO

THE FATE OF A NEOPROTEROZOIC INTRACRATONIC MARINE BASIN: TRACE ELEMENTS, TOC AND IRON SPECIATION GEOCHEMISTRY OF THE BAMBUÍ BASIN, BRAZIL

JOÃO PEDRO TORREZANI MARTINS HIPPERTT

Dissertação submetida à Banca Examinadora designada pelo Colegiado do Programa de Pós-Graduação em GEOLOGIA, como requisito para obtenção do grau de Mestre em GEOLOGIA, área de concentração GEOLOGIA ECONÔMICA E APLICADA.

Aprovada em 28 de junho de 2018, pela banca constituída pelos membros:

Prof. Fabrício de Andrade Caxito - Orientador
UFMG

Prof. Gabriel Jube Uhlein
UFMG

Prof. Isaac Daniel Rudnitzki
UFOP

Belo Horizonte, 28 de junho de 2018.

AGRADECIMENTOS

Agradeço ao universo por ter me encaminhado para este trabalho.

Agradeço aos meus Pais Vanize e João, meus irmão Daniel, Mariana e Rebeca pelo apoio, união e amor. Agradeço á Laura pelo amor, paciência, companheirismo e o apoio incondicional. Agradeço ao Nippon, Pequi (*in memorian*), Capivara e a Briggitte pelos momentos de descontração, alegria e pelo companheirismo.

Agradeço à Pró-Reitoria de Pós-Graduação (PRPG) da UFMG e ao programa de Pós-Graduação em Geologia do Instituto de Geociências (IGC) da UFMG pelo apoio à pesquisa.

Agradeço ao meu orientador Fabrício Caxito por ter me acolhido e acreditado em mim, e principalmente por ter me dado toda liberdade criativa e cronológica e para a realização desta dissertação. Agradeço também pela paciência e por toda a ajuda durante a realização deste mestrado.

Agradeço ao professor Hermínio Nalini por dar suporte a todas minhas análises laboratoriais, pelas discussões e pelo incentivo à realização de novas metodologias.

Agradeço à toda equipe do LgqA pelo suporte técnico. À Adriana por topar e apoiar à realização de uma metodologia complicada e trabalhosa, ao Léo por cuidar criteriosamente de todas as minhas análises e ao Celso pela ajuda na preparação de todos os tipos de amostras.

Agradeço ao Gabriel Uhlein pela ajuda em todas as etapas do mestrado e pelas inúmeras revisões do artigo e da dissertação.

Agradeço aos meus amigos Leonardo Gonçalves e Pedro Dieguez pelo incentivo, apoio e por todas as discussões científicas e filosóficas.

Agradeço ao financiamento da FAPEMIG pelos auxílios - APQ-00914-14, APQ-01711-14, PPM-00539-15 e PPM-00618-18.

Agradeço as mineradoras Ilcom Mineração Indústria e Comércio Ltda. e Holcim Brasil S.A. pelo acesso às amostras e áreas de estudo.

O presente trabalho foi realizado com apoio da Coordenação de Aperfeiçoamento de Pessoal de Nível Superior - Brasil (CAPES) - Código de Financiamento 001.

Abstract

Neoproterozoic marine systems are associated with major paleoecological changes that took place during the Ediacaran-Cambrian transition. During this timespan, the Bambuí basin located on east Brazil held a peculiar paleoenvironmental scenario. Due to its intracratonic evolution, the basin was partially disconnected from neighboring open marine systems. This isolated evolution rises a very interesting opportunity to understand how an isolated Neoproterozoic marine system evolved in contrast with regular open marine systems that ultimately evolved into the Cambrian Ecosystem. To understand the paleoenvironmental changes that took place in the Bambuí basin, we investigate the pre-glaciogenic deposits of Carrancas Formation and the post-glaciogenic mixed (Shale-Carbonate) successions of the Bambuí Group. Through the analysis of iron speciation, TOC, provenance, rare earthtrace elements data, and ^{13}C and ^{18}O analyses, our studies suggest a very complex environmental evolution. Firstly, our samples are marked by strong contamination of detrital continental material that can be related to an increased bioproductivity on both Carrancas Fm. and lower Bambuí group stratigraphic units, though provenance data show that all studied sediments probably share a common source rock, which likely changed the rare earth and trace elements contents of our samples. Iron speciation data, Ce anomalies and RSE enrichments shows that Lower Bambuí group stratigraphic units were likely deposited in an open marine scenario featuring high bioproductivity on shallow waters and euxinic incursions on predominant anoxic/ferruginous bottom waters. On the other hand, upper Bambuí stratigraphic units register a marine evolution in a restricted scenario, where anoxic ferruginous conditions probably reached surface waters. Finally, our data show that the lack of oceanic connection prevent the re-supply of marine sulfate, RSE, bionutrients such as Ba and ultimately of dissolved oxygen which may have decreased biological activity and probably damaged biological evolution, preventing the rise of a typical modern-like Cambrian ecosystem. In this sense, our data suggest that oceanic connectivity and proper re-supply of inorganic marine input were fundamental keystones in the development of complex life in the Ediacaran-Cambrian transition.

Keywords: Neoproterozoic-Cambrian transition; watermass restriction; redox sensitive element geochemistry; São Francisco basin; Neoproterozoic oxygenation

Resumo

Sistemas marinhos Neoproterozóicos estão associados a grandes mudanças paleoecológicas que ocorreram durante a transição Ediacarano-Cambriana. Durante esse período, a bacia de Bambuí, localizada no leste do Brasil, apresentava um cenário paleoambiental peculiar. Devido à sua evolução intracratônica, a bacia foi parcialmente desconectada des sistemas marinhos adjacentes. Esta evolução em um ambiente isolado, gera uma oportunidade muito interessante para entender como um sistema marinho Neoproterozóico isolado evoluiu em contraste com os sistemas marinhos regulares que em ultima analise evoluíram para o Ecossistema Cambriano. Para compreender as mudanças paleoambientais ocorridas na bacia do Bambuí, investigamos os depósitos pré-glaciogênicos da Formação Carrancas e as sucessões marinhas pós-glacialgênicas (Carbonato e folhelho) do Grupo Bambuí. Através da análise de especiação de ferro, TOC, estudos de proveniência , dados de elementos traços, terras raras e análises de 13C e 18O, nossos estudos sugerem uma evolução ambiental muito complexa. Primeiramente, as amostras estudadas são marcadas por uma forte contaminação de material continental detrítico que pode estar relacionado com uma bioprodutividade elevada nas amostras da Formação Carrancas e nas unidades basais do grupo Bambuí, embora os dados de proveniência mostrem que todos os sedimentos estudados provavelmente compartilham uma rocha fonte comum, o que provavelmente não alterou o conteúdo de terras raras e elementos traços das amostras. Dados de especiação de ferro, anomalias de Cério e o padrão de enriquecimento de RSE mostram que as unidades estratigráficas basais do Bambuí foram provavelmente depositadas em um cenário marinho aberto com uma alta bioprodutividade em águas rasas e incursões euxínicas em águas profundas predominantemente anóxicas / ferruginosas. Por outro lado, as unidades estratigráficas superiores do Grupo Bambuí registram uma evolução marinha em um cenário restrito, onde as condições ferruginosas e anóxicas provavelmente alcançaram águas superficiais. Finalmente, nossos dados mostram que a falta de conexão oceânica impede o reabastecimento de sulfato marinho, RSE, bionutrientes como Ba e, finalmente, de oxigênio dissolvido, que pode ter diminuído a atividade biológica e provavelmente danificado evolução biológica, impedindo a ascensão de um típico ecossistema cambriano. Neste sentido, nossos dados sugerem que a conectividade oceânica e o adequado reabastecimento de insumos marinhos inorgânicos foram pilares fundamentais no desenvolvimento da vida complexa na transição Ediacarano-Cambriano.

Palavras Chave: Transição Neoproterozóico-Cambriano; restrição marinha; geoquímica de elementos sensíveis a ox-redox (RSE); Bacia São Francisco ; oxigenação Neoproterozóica

LIST OF FIGURES

Fig. 1.1. A) Mo-U covariation plot from Algeo and Tribovillard (2009).B) Cd/Mo x Co/Mn covariation plots from Sweere et al. (2016). 5

Fig. 1.2. Ediacaran paleogeographical and tectonic context of the São Francisco Craton on southwest Gondwana from Reis & Suss, 2016. 10

Fig 1.3. Stratigraphic chart of the São Francisco Bambui Basin from Reis & Suss, 2016. 11

Fig 2.1. A) Ediacaran paleogeographical and tectonic context of the São Francisco Craton on southwest Gondwana, based on modern day continent configuration. After Misi et al. 2005 and Alkmim et al. 2006. B) Local geological context and localization of studied areas. C) Regional cross section showing São Francisco craton basement structure, filled by Bambuí basin deposits (not to scale). 18

Fig 2.2. Regional stratigraphic chart of São Francisco basin. Refs. - (1) Reis and Suss, 2016; (2) Vieira et al., 2007; (3) Caxito et al., 2012; (4) Paula Santos et al., 2014; (5) Warren et al., 2014; (6) Babinski et al., 2007; (7) Pimentel et al., 2012; (8) Reis, 2013 19

Fig 2.3. Stratigraphic placement of studied sections in the Bambui Basin column. All of the 35 samples analyzed for trace and REE geochemistry are shown in stratigraphic height on each local section. Regional Bambuí column was based on Reis & Suss, 2016. $\delta^{13}C$ data is from Reis, 2013. ...24

Fig 2.4. Broad view of studied sections. A) Carrancas section (1) located in a road (BR-040) outcrop Between Belo Horizonte and Sete Lagoas. B) Section 2 (Lower Sete lagoas Fm.), located at the Ilcom Quarry near Sete Lagoas. Truck at the right portion of the picture for scale. C) Section 4 (Serra de Santa Helena Fm.) at Papagaios quarry located in the city of Papagaios. D) Two different broad views (upper corner) from section 5 (Lagoa do Jacare Fm.), located at Jaíba. 26

Fig.2.5 A) Redox proxies results from all studied sections. B) Selected REE, Ba and CIA and stable isotope proxies from studied sections. Importantly, stratigraphic sections are in order, though not on stratigraphic continuity. 28

Fig. 2.6. Ternary major elements plots. A) Cao +Na2O-Al2O3+ K2O ternary plots, where the black arrow represent the normal chemical weathering trend from crustal materials (upper continental crust) towards clastic sediments (PAAS) from Taylor and McLennan (1985). Note that conversely, our samples moves from strongly weathered values towards less weathered samples (red arrow). B) Cao +Na_2O-Al_2O_3+ K_2O + FeO+MgO ternary plots. Black marks the chemical transition from Al rich samples (e.g Carrancas Fm.) towards samples with decreased Al contents and higher (Cao +Na2O+ Feo+MgO) (e.g Sete Lagoas, Serra de Santa Helena and Lagoa do Jacaré fms. 29

Fig 2.7. Provenance plots showing A) K_2O x Al_2O_3; B) Tio_2/Al_2O_3 x La/Yb; C) La/Th vs Hf source discrimination plots from Floyd and Leveridge (1987). D) TiO2 vs Zr source discrimination plots from Hayashi et al. (1997). Note that all provenance plots show low chemical variability (including carbonate samples on fig 2.7b), and point towards a common felsic igneous source (2.7c,d). 30

Fig. 2.8. Trace element cross plots (concentrations on ppm) between a) V,U,Mo and Ni X Zr on shale samples indicating low covariance of RSE with detrital elements (Zr) b) V,U,Mo and Cu x Zr on carbonates (Same as item a). c) VxU, VxMo, of shale and carbon showing strong covariations between these elements, suggesting a authigenic origin. D) Ba X Al and Ba x Zr plots of carbonates and shale samples against PAAS detrital average, showing that on both carbonate and shale samples, Sete Lagoas Formation presents enriched (Excess) Ba values, while Lagoa do Jacaré + Serra de Santa Helena fms. presents depleted Ba contents, which can be indicative of enhanced bioproductivity on lower Bambuí Basin stratigraphies. 31

Fig 2.9. PAAS (Taylor and McLennan, 1985) normalized REE plots from A) Carrancas Fm. B) Carbonates from Sete Lagoas Fm. C) Shales from Sete lagoas Fm. D) Carbonates from Lagoa do Jacaré Fm. E) shales from Serra de santa Helena Fm. F) shales from Lagoa do Jacaré Fm. 33

Fig 2.10 A) Mo-U covariation plot from Algeo and Tribovillard (2009). Carrancas Fm. plots featuring higher MoEF and Low UEF represent a typical marine evolution of a weakly restricted basin. While samples from Ilcom section falls on the suboxic evolution (low Mo and high U EF), Holcim section samples suggest an watermass evolution from weakly restricted towards watermass restriction. At last, Lagoa do Jacaré Fm.presents Low Mo and U EF which are caused by watermass strong restriction (See text for details) B) Cd/Mo x Co/Mn covariation plots from Sweere et al. (2016). 45

Fig 2.11. Probable paleogeographic (based on Misi et al. (2005) and Alkmim et al. (2006) and paleoenvironmental (this work) scenario of western Gondwana during the Cambrian-Ediacaran transition (i) Summarizes the environmental features of lower Sete Lagoas Fm. (Ilcom section). (ii) Summarizes the environmental features of middle Sete Lagoas Fm. (Holcim section) (ii) Represents the environmental scenario from upper Bambuí basin stratigraphies (Serra de Santa Helena and Lagoa do Jacaré Fm.). A) Following Neoproterozoic glaciations (i- Lower Sete Lagoas Fm.), western Gondwana basins were liked connected by continental seaways (Tohver et al., 2010, 2012; Warren et al., 2014; Paula-Santos et al., 2017), which were related to appearance of *cloudina sp.* and typical open marine environments that can be observed on middle Sete Lagoas Fm. (ii). B) During the Ediacaran-Cambrian transition, these seaways were disconnected by tectonic activity, isolating the São Francisco Basin, which evolved in a restricted environmental scenario as suggested by Lagoa do Jacaré Fm. data (iii). .47

SUMMARY

INITIAL CONSIDERATIONS 10
CHAPTER ONE 11
1.1) The Neoproterozoic-Phanerozoic transition 11
1.2) Neoproterozoic black shale geochemical proxies 12
1.2.1 Major and Trace Element Data 12
1.2.2 Redox Sensitive Elements (RSE) geochemistry 14
1.2.3 Iron speciation technique 15
1.2.4 Neoproterozoic carbonate rare earth element geochemical proxies 15
1.3) Previous studies and open questions 16
1.4) Local geological context 17
1.4.1 Stratigraphy and depositional environments 17
1.4.2 Tectonic evolution 19
1.4.3 Depositional ages 20
1.4.4 δ^{13}C and δ^{18}O data 21
1.4.5 Rare earth element data 21
CHAPTER TWO - (MANUSCRIPT - THE FATE OF A NEOPROTEROZOIC INTRACRATONIC MARINE BASIN: TRACE ELEMENTS, TOC AND IRON SPECIATION GEOCHEMISTRY OF THE BAMBUÍ BASIN, BRAZIL) 22
2.1) Introduction 22
2.2) Geological background 25
2.3) Material and Methods 29
2.4) Results 31
2.5) Discussion 44
2.5.1 Provenance, detrital input and marine productivity 44
2.5.2 Redox conditions 47
2.5.3 Bambuí basin paleoenvironmental evolution 49
2.5.4 Paleoenvironmental implications for Neoproterozoic intracontinental basins 54
2.5) Conclusions 56
REFERENCES 58

INITIAL CONSIDERATIONS

This work was submitted to the postgraduate board of the Instituto de Geosciencias (IGC) in partial fulfillment of the requirements for the degree of Master of science in geochemistry at the Universidade Federal de Minas Gerais (UFMG). The work is based on the data acquired between March 2016 and March 2018, which is focused on the multi-proxy geochemistry of shale and carbonate samples from Bambuí Basin.

This thesis is divided into two chapters. The first chapter consists of introductory concepts including background, methodologies and previous studies analysis. The second chapter exhibits the results of this work presented in a manuscript form. Following the Msc guidelines, this manuscript was submitted to the international scientific journal *Chemical geology*, as a pre-requisite for the submission of this dissertation.

CHAPTER ONE

1.1) The Neoproterozoic-Phanerozoic transition

The Neoproterozoic-Phanerozoic transition is marked by drastic changes on both biological and geochemical record. Biologically, the Neoproterozoic period is marked by the appearance of diverse, large shelly animals after the Marinoan glaciation, and is commonly represented by typical terminal Ediacaran (550-542 Ma) trace fossils such as *cloudina sp.* and *kimberella* (Och & Shields-Zhou, 2012). This Ediacaran fauna is extinguished at 542 Ma, with the appearance of the trace fossil *Treptichnus pedum* and the rise of far complex life forms of the Cambrian Fauna (Och & Shields-Zhou, 2012).

This drastic biological and evolutionary Neoproterozoic- Phanerozoic changes are followed by several geochemical swifts in the sedimentary record. The $\delta^{13}C$ for example, is marked by strongly negative pulses (up to -10‰) of the Shuram-Wonaka anomaly during midle Ediacaran which evolve to oscillant values of $\delta^{13}C$ around 0‰ on terminal Ediacaran (Halverson et al., 2010). The explanations of this $\delta^{13}C$ oscillations are very controversial, and most likely caused deep ocean oxygenation (Och & Shields-Zhou, 2012). The $^{87}Sr/^{86}Sr$ record also presents strong swifts druing the Ediacaran rising from low (< 0.7060) $^{87}Sr/^{86}Sr$ values following the Marinoan glaciation rising up to high (up to 0.7090) on terminal Ediacaran (Halverson et al., 2010), which are generally interpreated as the result of enhanced continental silicate wheatering (Och & Shields-Zhou, 2012).

Even more controversial Ox-Redox proxies also characterize the Neoproterozoic-Phanerozoic transition. While, Ce*/Ce anomalies and iron speciation data suggests that the Neoproterozoic ocean presented a stratified structure featuring a superficial oxic layer and bottom anoxic/ferruginous layer (Poulton & Canfield, 2011), redox sensitive elements (RSE), $\delta^{34}S$ and $\delta^{53}Cr$ data suggests a protracted atmospheric oxygenation event during late Ediacaran (Li et al., 2010; Johnston et al., 2010; Frei et al., 2011), though this protracted oxygenation was only momentarily reached on Neoproterozoic deep seawater (Poulton & Canfield, 2011). Furthermore, contrasting RSE and iron speciation data from Miller et al. (2017) suggests that this protracted atmospheric oxygenation may be not evident on every Ediacaran sedimentary sequence, and most likely, the atmospheric oxygenations events occurred rather locally than globally.

Further, the Neoproterozoic-Phanerozoic transition is one of the most complex and intriguing time spans, where strong interactions between supercontinent amalgamation, atmospheric

oxygenation and seawater chemical evolution culminate in a new biological and evolutionary trend (Och & Shields-Zhou, 2012). In this scenario, the Bambuí basin places itself as one of the most poorly understood remnants of Southern Gondwana, as only extremely recent contributions (e.g Warren et al., 2014; Caxito et al., 2012, 2018; Paula Santos et al., 2015, 2017, 2018; Uhlein et al., 2017) tried to establish a comprehensive correlation between typical Neoproterozic features (Supercontinent amalgamation, post glaciogenic activity, atmospheric oxygenation and continental weathering, seawater ox-redox structure, and biologic evolution) on Bambuí Basin stratigraphy.

Following the recent achievements made on Bambuí Basin, this contribution explores new (first time on Bambuí Basin) multi-proxy geochemical data in order to establish a strong and comprehensive correlation between tectonic activity, atmospheric oxygenation, seawater ox-redox switch and biological evolution that took place during the Neoproterozoic-Phanerozoic on Bambuí basin.

1.2) Neoproterozoic Black Shale Geochemical Proxies

In this section, the interpretative framework of the selected geochemical proxies that were applied in this study are presented as follows:

1.2.1. Major and Trace Element data

Provenance

The chemical index of alteration (CIA) is used to understand the influence of protolith weathering on sediment geochemistry and track major element variability of source rock, where CIA = [Al_2O_3 / (Al_2O_3 + CaO*+Na_2O+K_2O)] * 100, introduced by Nesbitt & Young (1982). CaO* is referred to the CaO content of the detrital fraction, meaning that all the CaO content from carbonate minerals and phosphate phases should be excluded from the equation. Normal tropical weathering regimes yield sediments with CIA values around 75-80 (PAAS values around 72-75). These values tend to decrease in sediments influenced by colder and/or drier weather regimes (Lower Al2O3 and higher CaO*+Na_2O+K_2O concentrations), and to increase on strong weathering regimes (e.g. modern suspended mud sediments from the Niger river with CIA values around 95). Complementing CIA values, shale major elements (K, Al and TI) are also commonly plotted against common provenance tracers such as La, Sc, Th, Zr and Co as those trace elements are associated with siliciclastic phases and are also relatively immobile during diagenesis and authigenic enrichment processes (Tribovillard et al., 2006). Additionally, La/Sc and Zr/Sc ratios and Co contents are commonly used as proxies for igneous differentiation processes which can also be used to evaluate sediment provenance (Zhai et al., 2018).

Marine Restriction Evaluation

Recent contributions used the covariation of trace and major elements registered in modern sediments to understand seawater circulation dynamics in different settings. Based on Mo-U covariation Algeo and Tribovillard (2009) established common enrichment patterns of marine seawater which are directly related to watermass circulation and restriction. By cross plotting U and Mo enrichment factors (EF) against normal seawater U/Mo concentrations, it is possible to qualitatively estimate seawater evolution and interpret possible sedimentary environments (fig. 1.1 A). In modern open marine settings for example, the absence of euxinic bottom waters promotes higher U over Mo enrichment factors, while open marine settings featuring bottom water euxinia tend to present sediments with Mo/U ratios similar to modern seawater. If the oceanic connection is lost, and watermass restriction is configured, Mo enhanced uptake without re-supply tend to shift Mo-U plots towards Higher U(EF) values. These plots have been successfully applied to innumerous contributions on both modern and ancient marine sediments (e.g Deni et al., 2014, Zhou et al., 2015, Ma et al., 2017). Importantly, other redox (e.g iron speciation) proxies are necessary to complement U-Mo(EF) plots in order to provide an outside redox parameter, elucidating their interpretation.

In the same way, Sweere et al. (2016) utilized a very similar data set from modern sediments to establish Cd/Mo x Co/Mn covariation patterns. As Co and Mn present similar enrichment patterns on marine sediments, is possible to discriminate upwelling and restricted marine settings based on Co x Mn plots (fig. 1.1 B). According to Sweere et al. (2016), Co and Mn input in open marine settings are only related to upwelling currents which transport these elements from bottom waters, limiting their enrichments on sediments. Conversely, restricted and stagnant settings are fueled by riverine and crustal input of Mn an Co, elevating the concentrations of these elements in the water column. Restricted basins are also associated with water column stratification and anoxia, which are believed to also lead to authigenic sediment enrichment of both Mo and Mn. Complementary, Cd/Mo ratios are used to constrain the whole of organic carbon production in the water column. Although the use of Cd/Mo ratios may be limited in our samples as Mo enrichments are remarkably poorly on typical ferruginous Neoproterozoic settings.

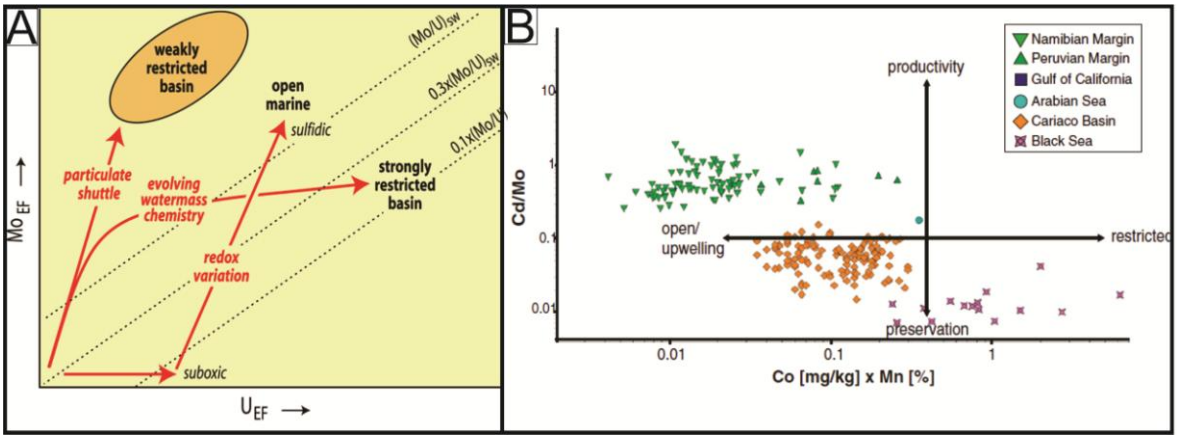

Fig. 1.1. A) Mo-U covariation plot from Algeo and Tribovillard (2009).B) Cd/Mo x Co/Mn covariation plots from Sweere et al. (2016).

1.2.2. Redox Sensitive Elements (RSE) geochemistry

Combined Redox sensitive elements (RSE) enrichments of U, Mo, and V are very robust proxies used to constrain variations in the redox condition of sedimentary environments (Algeo and Maynard, 2004, Och & Shields-Zhou, 2012; Sperling et al., 2013). The mechanisms of enrichment of these elements are very complex (Review by Tribovillard, 2006), and varies for each redox sensitive element. These elements are leached from crustal sources through oxidative weathering and transported by riverine influx into marine basins. In oxic watermass conditions, Mo is found as molybdate (MoO_4^{2-}) (Broecker and Peng, 1982). Nevertheless, if sulfide {H2S(aq)} concentration is above 10µM, molybdate switches to tetrathiomolybdate ($MoOxS^{4-}x$), a reactive particle which facilitates Mo scavenging by organic matter and sulfide minerals (Erickson & Helz, 2000). In order to authigenically enrich Mo, euxinic conditions are necessary in the watermass, which should also have enough supply of oxidate Mo in the form of molybdate (Scott and Lyons, 2012).

U(VI) is found as the uranyl carbonate anion ($UO_2(CO_3)_3^{4-}$) in oxic watermass, where it is reduced back to U(VI) and precipitated as UO_2, U_3O_7 or U_3O_8 if mildly anoxic conditions are reached. Furthermore, U(VI) reduction and authigenic enrichment is also linked with the formation of organic-metallic ligands with humic acid and absorption onto ferric iron hydroxides directly in the sediment, if anoxic conditions are prevalent (Klinkhammer and Palmer, 1991). Unlike Mo, U authigenic enrichments are not dependent on sulfide availability (Tribovillard et al., 2006), and are rather associated with total organic carbon (TOC) contents (McManus et al., 2005). V is found as vanadate ion species (HVO_4^{2-} and H_2VO^{4-}) on modern oxic seawater. If anoxic (mildly euxinic)

water conditions are reached, V(V) is reduced to V(IV) and removed from the water column by the formation of organic-metallic ligands and adsorption. Experimental studies suggest that in strongly euxinic conditions V(IV) is further reduced to V(III), increasing V authigenic enrichments (Wanty and Goldhaber, 1992). These findings, however, are in conflict with modern natural highly euxinic settings where V is retained in the water column due to organic ligand complexation and other chemical processes (Algeo and Maynard, 2008). Thus, V is expected to be authigenically enriched in anoxic (non euxinic) settings, though the persistence of strongly euxinic conditions may lead to anomalous enrichment patterns (Scott et al., 2008).

1.2.3. Iron Speciation technique

Iron speciation data is one of the most reliable Redox proxies, which is widely used in modern and ancient sediments. The method consists of a sequential extraction scheme introduced by Poulton and Canfield (2005,2011), which separates two distinct iron pools. The first pool consist of highly reactive iron minerals (FeHr), which comprises phases that are available for reductive dissolution and consists of FeCarb (Fe in carbonate minerals such as siderite and ankerite), FeOx (Fe in Fe(III) valence such as in goethite and hematite), FeMag (comprising mixed valence Fe minerals as magnetite) and FePy (Comprising Fe associated with sulfides, mainly pyrite), where the sum of all phases yield the total highly reactive iron pool (FeHr = FeCarb + FeOx + Fe Mag + FePy). The second pool consists of the total Fe content (FeT) and is composed by the sum of unreactive silicate iron pool (FeU) and highly reactive iron pool (FeHr). It follows that if FeHr/FeT > 0.38 anoxic conditions are interpreted, if FePy/FeHr > 0.7 euxinic conditions were predominant in the water column, whereas if FePy/FeHr < 0.7 ferruginous conditions are interpreted (Raiswell and Canfield, 1998, Poulton and Canfield, 2011). Nevertheless, modern oxic sediments are deposited with an average of FeHr/FeT = 0.22, suggesting that $0.22 < FeHr/FeT < 0.38$ values may indicate both oxic or anoxic conditions (Poulton and Canfield, 2011). These intermediate values are reached due to mass balance calculations that dictate that not every anoxic sample should have high FeHr values (Poulton and Canfield, 2011). In this case, the use of FeT/Al ratios is recommended to address Fe enrichment (Lyons and Severmann, 2006).

1.2.4. Neoproterozoic Carbonate Rare earth element Geochemical Proxies

Cerium is the only REE which can track redox variations on marine systems from chemical sedimentary rocks (Bau and Alexander, 2006). Ce(III) oxidation to Ce(IV) and consequent scavenging is controlled by the presence of Mn and Fe oxides, which occurs under oxic conditions and produces negative (normalized to PAAS) anomalies. In the presence of anoxic conditions, Fe-Mn oxides are solubilized and Ce(III) behaves as all other REE, producing positive or no Ce

anomalies (Bau & Dulski, 1996; Frimmel, 2009; Li et al., 2010; Wallace et al., 2017). Post-depositional processes and diagenesis are not likely to alter Ce relative concentrations against other REE (Banner et al., 1988; Shields and Stille, 2004; Webb et al., 2009) and Ce anomaly values are believed to register the overall redox balance of the marine system, rather than local variations (German and Elderfield, 1990; Frimmel, 2009; Wallace et al., 2017).

While Ce is used to trace redox chemistry, $\sum \mathrm{REE} + \mathrm{Y}$ and Y/Ho are used to constrain crustal detrital contamination on carbonatic rocks. As the sum of $\sum \mathrm{REE} + \mathrm{Y}$ on pure carbonates are expectably low, enrichments in these values are a strong indicative of contamination by hydrothermal or crustal particulate material (Frimmel, 2009). Y/Ho ratios present values around 60-90 on modern open marine seawater (Lawrence et al., 2006). Any deviations below these values are thought to be related to mixing with riverine and ultimately crustal components, as crustal Y/Ho ratios ~27 (Taylor and McLennan, 1985, Kamber et al., 2005). As Ho is believed to be removed from the water column twice as fast as Y due to differences on surface complexation behavior (Nozaki et al., 1997), Y/Ho ratios are believed to be a very useful proxy to register seawater contamination by continental parcticulate input (Frimmel, 2009). Light REE (LREE), Middle REE (MREE) and Heavy REE (HREE) contents are also analyzed on carbonate samples to constrain seawater mixing (Frimmel, 2009). According to Lawrence et al. (2006), as opposed to riverine water which presents depleted MREE and HREE contents, seawater tends to present MREE and HREE enrichment over LREE.

1.3) Previous studies and open questions

Since pioneer works from Costa & Branco (1961), Almeida (1977) and Dardene (1978), the evolution of Bambuí basin has been a matter of a intense and dynamic debate. While works from 1980's to 1990' focused on the description and classification of Bambuí basin stratigraphy (e.g Rocha-Campos and Hasui, 1981; Karfunkel & Hoppe, 1988), contributions from 1990`s to early 2000`s started to explore evolving geochemical proxies including $\delta^{13}\mathrm{C}$ and $\delta^{18}\mathrm{O}$ data (e.g Iyer et al., 1995; Santos et al., 2000; Alvarenga et al., 2007) and Pb/Pb and U/Pb geochronology (e.g Babinski et al., 1999, 2007). Also during late 1990`s and early 2000`s, several works proposed diverging depositional tectonic frameworks for Bambuí basin stratigraphies (e.g Dardenne, 2000; Alkmim & Martins-Neto, 2001; Martins & Lemos, 2007).

Recently however, a growing number of contributions are exploring diverse geochemical and stratigraphic features of Bambuí basin. For example, diverse works tried to establish a robust depositional age for Bambuí group deposits based on refined U/Pb and Pb/Pb geochronology (e.g Pimentel et al., 2011; Paula-Santos et al., 2015 ; Caxito et al., 2018) and paleontology (Warren et

al., 2014). In addition, several works also focused on expand $\delta^{13}C$, $\delta^{18}O$ and $^{87}Sr/^{86}Sr$ data (e.g Caxito et al., 2012, 2018; Paula Santos et al., 2015, 2017; Uhlein et al., 2017), while some works focused on the depositional tectonic framework of Bambuí Basin (Alkmim & Martins-Neto, 2012; Reis & Suss, 2016; Uhlein et al., 2016,2017).

Nevertheless, only a few recent contributions focused on Major, Trace and rare earth element data (e.g Uhlein et al., 2016; Kuchenbacker et al., 2016; Caxito et al., 2018; Paula Santos et al., 2018), which is reflected in a still poorly explored ox-redox and paleoenvironmental picture of the Bambuí Basin depositional environment. This scenario is also corroborated by the lack of studies carried on shale samples coupled to the absence of data from modern geochemical proxies such as Iron speciation and Total Organic Carbon (TOC).

Due to the lack of this data, questions regarding the paleoenvironmental evolution of Bambuí basin such as the evolution of Ox-redox conditions, the whole of continental oxygenation and Biological production still unanswered. Thus, in this scenario this contribution explores multi-proxy geochemistry on Bambuí basin stratigraphy, in order to fulfill a poorly explored paleoenvironmental threshold.

1.4) Local geological context

1.4.1. Stratigraphy and depositional environments

The São Francisco Basin is located in eastern central Brazil and covers Paleo-proterozoic to Archean basements rocks of its homonym Craton. The basin's stratigraphy is marked by a lower clastic-alluvial unit of Mesoproterozoic age named Espinhaço Supergroup which is superposed by Neoproterozoic pre-glaciogenic and glaciogenic units and a post-glaciogenic mixed carbonatic-siliciclastic group named Bambuí Group (Alkmim & Martins-Neto 2001, 2012- figs 1.2 and 1.3).

This work focus on the Neoproterozoic portion of the São Francisco Basin, encompassing both pre-glaciogenic and post-glaciogenic units, here referred to as the Bambuí Basin following Dardenne (1978). The Jequitaí Formation is the main representant of glaciogenic activity in the southern portion of the São Francisco Basin, and is composed of typical diamictites, shales and local striated pavements (Isotta et al., 1969; Karfunkel et al., 2002; Cukrov et al. 2005). Temporarily associated with the Jequitaí Formation, the Carrancas Formation is found on small basement troughs along the São Francisco Basin margins presenting a maximum thickness of 80-100m (Uhlein et al., 2016). This unit is also characterized by diamictites, shales and pink carbonates, though its origin may not be related to glaciogenic activity (Uhlein et al., 2016). Some

early workers suggested that Carrancas Formation was related to Jequitaí Formation as an associated glaciogenic deposit (Costa and Branco, 1961; Martins-Neto et al., 2001; Reis and Alkmim, 2015), though recent evidences suggest that Carrancas Formation deposition was controlled by gravitational processes in a pre-glaciogenic open marine setting (Uhlein et al., 2016).

The Bambuí Group deposits overlay these glaciogenic units in sharp abrupt contacts, which can be also observed in onlapping geometries when the sediments are in direct contact with basement rocks (Vieira et al., 2007). The Bambuí Group is composed of thick (over 1000m) mixed carbonate and siliciclastic sediments. These sediments are disposed in three shallowing upwards megacycles, which are included in a general shallowing upwards trend (Dardenne, 1978; Alkmim & Martins-Neto, 2012). The base of the group is represented by the Sete Lagoas Formation, which presents a shallowing upwards trend and is composed by a majority of carbonatic rocks alternated with minor shale layers presenting a maximum thickness of 500m (Vieira et al., 2007). The unit is composed by a bottom member characterized by pink dolomites and pelitic rocks which is strongly influenced by post-glaciogenic activity in a restricted shallow marine setting (Vieira et al., 2007; Caxito et al., 2012; Paula-Santos et al., 2015). This member is overlayed by typical open marine deposits featuring homogeneous thinly layered platform carbonates (Vieira et al., 2007). The top portion of Sete Lagoas Formation is composed of shallow platform carbonates featuring coarse-grained stromatolitic carbonatic rock with subaerial exposition and abundant ooliths.

The second shallowing upwards comprises Serra de Santa Helena and Lagoa do Jacaré Formation (Alkmim & Martins-Neto, 2012- fig. 1.3). Serra de Santa Helena Formation is homogeneously composed of deep marine shales and episodic carbonatic rock lenses (Maximum thickness of 640m). In turn, Lagoa do Jacaré Formation (maximum thickness of 350m) is composed by a large variety of shallow platform carbonatic rocks featuring Coarse-grained stromatolites, oolites and calci-lutites alternated with thin shale layers, which are interpreted to be deposited in a restricted marine setting (Reis, 2013; Paula-Santos et al., 2017). The top of the Bambuí Group stratigraphy is represented by the last shallowing upwards megacycle and comprises Serra da Saudade and Tres Marias formations (maximum thickness of 100m for both units). The Serra da Saudade Formation is represented by siliciclastic shallow platform deposits featuring shales and sandstones, whereas Tres Marias Formation is represented by alluvial arkoses and conglomerates (Chiavegatto et al., 2003)

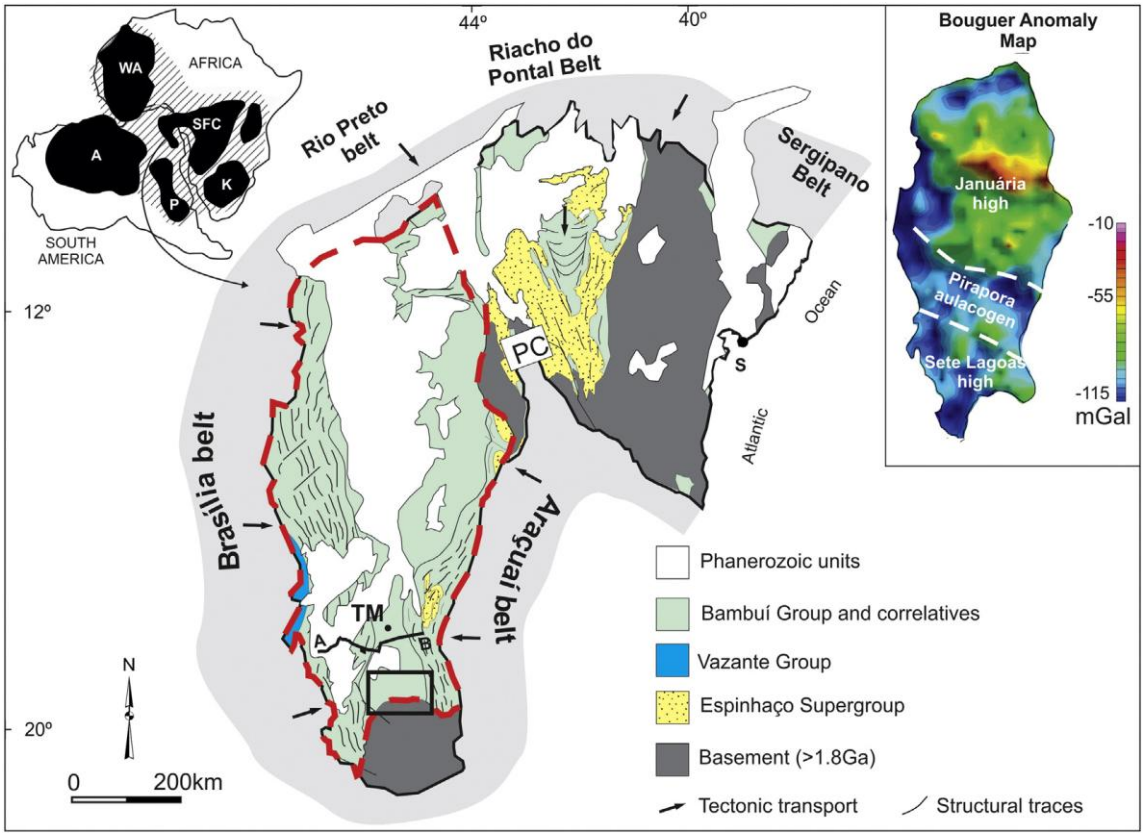

Fig. 1.2. Ediacaran paleogeographical and tectonic context of the São Francisco Craton on southwest Gondwana from Reis & Suss, 2016.

1.4.2. Tectonic evolution

The most classical interpretations suggest that the infilling of Bambuí Basin represents a typical foreland cycle generated by the development of thrust fronts at the Brasilia belt located in the western margin of São Francisco Craton (Alkmim & Martins-Neto, 2001). Although, the presence of a seismic discontinuity on lower Sete Lagoas Fm. suggests that the Bambuí Group deposition may be related to two discontinuous depositional events (Martins & Lemos, 2007). As proposed by Uhlein et al. (2017), this unconformity may be related to the formation of a foreland flexure as a result of foredeep subsidence and forebulge uplift during increasing orogenic load on the Brasilia belt. In this model, this flexure may have led to a depositional hiatus, separating a lower and older unit from the rest of Bambuí basin stratigraphy, which represents a typical foreland cycle (Reis & Suss, 2016; Uhlein et al., 2017- fig. 1.3).

Importantly, this seismic discontinuity is not always observable on stratigraphic and isotopic records, and despite its regional implications, these tectonic models do not clarify the environmental depositional conditions of Bambuí sediments, which suggests that the paleoenvironmental evolution

of Bambuí basin was also influenced by internal biogeochemical processes in addition to regional controls.

1.4.3. Depositional ages

The depositional age of Bambuí Basin still a matter of a intense debate. Initial geochronological insights from whole-rock Pb/Pb isochrons on lower Sete Lagoas Formation carried by Babinski et al. (2007) yield 740 Ma, thus implying a Sturtian age for Lower Sete Lagoas Formation. Although, recent detrital zircon U/Pb geochronology conducted by Pimentel et al. (2011) and Paula-Santos et al. (2015) recovered from the middle portion of Sete Lagoas Formation, yield minimum depositional ages of 630-610 Ma and 592-557 Ma respectively. This data is in concordance with recent paleontological evidence from Warren et al. (2014), which recovered a terminal Ediacaran index fossil *cloudina sp.* from middle Sete Lagoas Fm. which suggests a depositional age of 550-542 Ma.

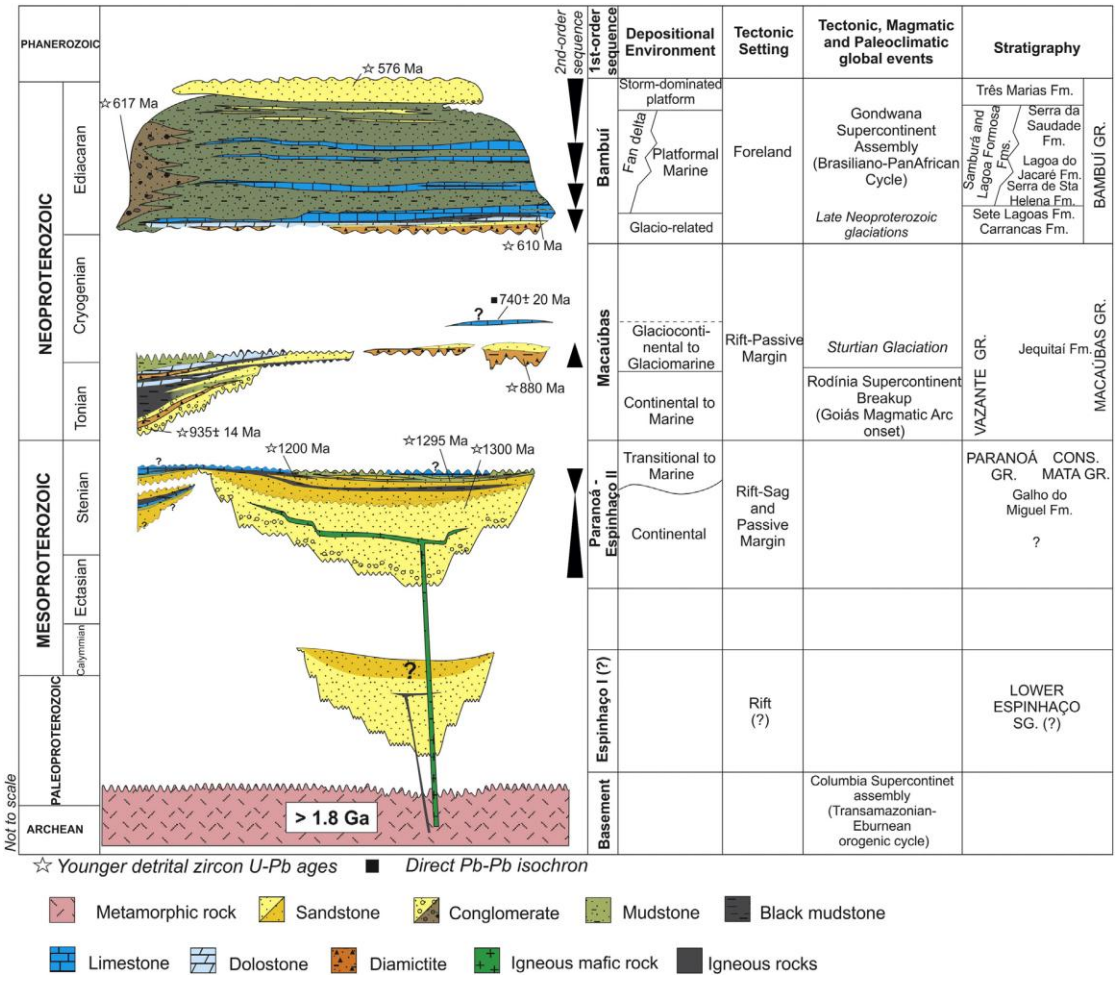

Fig 1.3. Stratigraphic chart of the São Francisco Bambui Basin from Reis & Suss, 2016.

In addition, Caxito et al. (2018) obtained a carbonate whole-rock Pb/Pb isochron age of 608 Ma on lower Sete Lagoas Formation. This age and $\delta^{13}C$, $\delta^{18}O$ and $^{87}Sr/^{86}Sr$ data from Caxito et al. (2012), suggests that in fact, lower Sete lagoas Formation carbonates may represent a typical post-Marinoan cap carbonate. This apperently contrasting ages were organized by Uhlein et al. (2017) and caxito et al. (2018) which suggest that a major unconformitty (see section 1.2.2) separates a lower post-Marinoan (630-560Ma) cap carbonate unit from a Ediacaran (550-542Ma) carbonate unit which encompasses midle and upper sections of Sete Lagoas Formation.

1.4.4. $\delta^{13}C$ and $\delta^{18}O$ data

The $\delta^{13}C$ and $\delta^{18}O$ record of Bambuí Basin is well documented specially on Sete Lagoas Formation. Classically, the $\delta^{13}C$ and $\delta^{18}O$ records starts at increasingly negative upwards values on lower cap carbonates where $\delta^{13}C$ goes from -3‰ to 4.5‰ and $\delta^{18}O$ goes from -4.5‰ to -6.5‰ (Alvarenga et al., 2007; Caxito et al., 2012). This lower cap carbonate unit is overlayered by a homogeneous thin laminated limestones which features decreasing $\delta^{13}C$ values from -4‰ to around -1‰, stabilizing around 0‰ and $\delta^{18}O$ values around -4‰ . The upper portion of Sete Lagoas Formation can present different $\delta^{13}C$ values which can remain on 0‰, or gradually increase to positive values up to 4‰ (Santos et al., 2000; Alvarenga et al., 2007; Vieira et al., 2007) or even 8‰ in some locations (Martins & Lemos, 2007).

Contrastingly, Lagoa do Jacaré Formation $\delta^{13}C$ and $\delta^{18}O$ data is still very scarce on recent literature. Nevertheless, data from Santos et al. (200), Reis (2013) and Paula-Santos et al. (2017) points towards a homegeneous isotopic composition featuring extremely positive $\delta^{13}C$ values ranging between 10‰ and 15‰ and $\delta^{18}O$ values around -10‰ and -5‰.

1.4.5. Rare earth element data

Rare earth element (REE) data is also scarce on Bambuí Basin, though recent contributions start to explore rare earth element variability on Bambuí Basin carbonates (Kuchenbecker et al., 2016; Caxito et al., 2018; Paula-Santos et al., 2018). The REE signature of Bambuí Basin is remarkably affected by continental (Shale component) contamination, which is represented by decreased, low Y/Ho ratios close to crustal averages (ca. 27-40) , and flattened REE normalized to Post Australian Archean Shale (PAAS) (Taylor & McLennan, 1985) patterns on REE plots (Kuchenbecker et al., 2016; Caxito et al., 2018; Paula-Santos et al., 2018). Although, in some portions of the basin, normal REE normalized to PAAS Neoproterozoic signatures and typical

seawater Y/Ho ratios (ca. 40-60) were observed by Caxito et al. (2018) on middle Sete Lagoas Formation and on Upper Lagoa do Jacaré Formation by Paula-Santos et al. (2018).

Ce/Ce* anomalies are also weakly explored on Bambuí Basin stratigraphy. Caxito et al. (2018) obtained negative (between 0.7 and 0.9) Ce/Ce* anomalies on lower Sete Lagoas Formation, while Vieira, (2007) and Paula-Santos et al.(2018) obtained positive Ce/Ce* anomalies on middle Sete Lagoas and Lagoa do Jacaré formations carbonates.

CHAPTER TWO - (MANUSCRIPT - THE FATE OF A NEOPROTEROZOIC INTRACRATONIC MARINE BASIN: TRACE ELEMENTS, TOC AND IRON SPECIATION GEOCHEMISTRY OF THE BAMBUÍ BASIN, BRAZIL)

2.1) Introduction

Marine systems are thought to be the warehouse of dramatic climate, biologic and chemical changes that took place during the Neoproterozoic - Paleozoic transition which ultimately led to the Cambrian explosion of complex life (Knoll, 2000; Hoffman & Schrag, 2002; Canfield et al., 2007; Scott et al., 2008; Och & Shields-Zhou, 2012; Sperling et al., 2013; Li et al., 2013; Wallace et al., 2017; Caxito et al., 2018). This biological transition was strongly influenced by highly complex and dynamic Neoproterozoic environments which were affected by glaciogenic periods, seawater redox variation, the rise of atmospheric oxygen levels, and tectonic changes among many other factors (Collins and Pisarevsky, 2005; Conway Morris, 2006; Sperling et al., 2013; Li et al., 2013; Wallace et al., 2017).

Unlike modern marine systems, the majority of Neoproterozoic settings are distinguished by a stratified watermass with an upper oxygenated layer with abundant biological activity separated by a chemocline from a bottom layer where organic matter from surface sinks and causes anoxia (Guo et al., 2007; Scott et al., 2008, Shen et al., 2010; Guo et al., 2016; Miller et al., 2017). While this upper layer tends to register oxic conditions (e.g negative Ce anomalies), the bottom layer is commonly responsible for Redox Sensitive trace Element (RSE, such as U, V, and Mo) enrichment that indicates widespread anoxia (Algeo, 2004; Sahoo et al., 2012).

Whereas highly sulfidic (euxinic) settings were widespread on the Mesoproterozoic era, ferruginous conditions are thought to have dominated bottom water oxi-redox chemistry of Neoproterozoic seawater (Canfield et al., 2008; Johnston et al., 2010; Guilbaud et al., 2015). Recent evidence for this hypothesis arises from an increasingly large dataset of iron speciation results, which firmly track redox variations based on dissolved iron pool ratios (Poulton and Canfield, 2005, 2011). Furthermore, iron speciation data suggests that quick and short euxinic pulses are often introduced into this predominantly ferruginous marine setting (Johnston et al., 2010). This complex redox evolution is also reflected on the RSE record of Neoproterozoic basins, which ranges from highly (over 1000 ppm) to negative (below average shale values) RSE enrichment on arguably contemporaneous basins (Sahoo et al., 2012; Miller et al., 2017). Hypothesis for explanation of high RSE enrichment includes the rise of continental oxidative weathering (Sahoo et al., 2012), prolonged euxinic periods (Lyons et al., 2009) and high organic carbon burial rates (Johnston et al.,

2010), while low enrichment or depletion has been attributed to low local RSE reservoirs (Miller et al., 2017), ineffective atmospheric oxygenation and/or possible reduced authigenic uptake rates on ferruginous settings (Johnston et al., 2010; Miller et al., 2017).

Besides their highly complex redox evolution, Neoproterozoic marine basins are also affected by enhanced continental particulate input that strongly affected Rare Earth (REE) and trace element signatures of carbonatic rocks (Frimmel, 2009; Rodler et al., 2016; Li et al., 2017; Caxito et al., 2018). These variations are characterized by a sharp increase of REE concentrations following shale distribution, leading to flattened REE normalized to PAAS (Post Archean Australian Shale; Taylor and McLennan, 1985) signature, and to decreased Y/Ho values close to the crustal average (ca. 25-27) (Frimmel, 2009). This Neoproterozoic detrital (continental) contamination is interpreted as a direct result of enhanced continental detrital influx (Li et al., 2017) which may be caused by several factors such as protracted deglaciation melt water runoff (Hoffman & Schrag, 2002), detrital input from adjacent upwelling areas such as active orogens and traphrogens (Cox et al., 2016; Rodler et al., 2016), and possibly enhanced continental oxidative weathering (Sahoo et al., 2012). Beyond abnormal REE fractionation patterns of carbonates, enhancing continental detrital input are also related to the transport of 13C-depleted organic carbon and inorganic detrital component to Neoproterozoic marine basins during deglaciation and melt water runoff (Hoffman and Schrag, 2002). In many cases, this enhanced influx of continental material (which is not necessarily related to post-glaciogenic periods) is also accounted to transport bio-nutrients such as Ba, Co, Cd and Mn from local source areas (Cox et al., 2016), promoting an increase in local bioproductivity (Ma et al., 2017), which increases organic carbon burial and promotes biological diversification (Och & Shields-Zhou, 2012).

The Bambuí basin (Eastern Brazil) in West Gondwana held remnants of at least one major Neoproterozoic glaciation, represented by glacially related diamictites of the Jequitaí Formation deposited on top of striated pavements, and associated shallow to deep marine deposits of the Bambuí Group and Carrancas Formation (Karfunkel et al., 2002; Cukrov et al. 2005; Vieira et al., 2007 ; Alkmim & Martins-Neto, 2012; Caxito et al., 2012, 2018; Uhlein et al., 2016, 2017). Apart from glaciogenic activity, this time span was also a period of intense crustal reworking and orogenic build-up at the São Francisco Craton margins, which strongly affected the detrital charge of the Bambuí Basin (Pimentel et al., 2011; Caxito et al., 2012; Kuchenbecker et al., 2016; Paula-Santos et al., 2017). More interestingly, the Bambuí Basin is thought to be formed inside an intracratonic setting, surrounded by contemporaneous Neoproterozoic orogens (Alkmim and Martins-Neto, 2001; Caxito et al., 2012; Paula-Santos et al., 2017), which may have prevent effective seawater connection with outer open marine settings (Martins et al., 2007; Santos et al., 2000, Paula-Santos

et al., 2017). This peculiar environmental scenario is very attractive, in order to understand how an isolated Neoproterozoic environment evolved, opposed to regular open marine Neoproterozoic systems which ultimately evolved into the Cambrian marine systems. Although some major progress was recently made on the understanding of São Francisco Basin evolution (Caxito et al., 2012, 2018; Warren et al., 2014; Paula-Santos et al., 2014, 2017, 2018; Reis & Suss, 2016; Uhlein et al., 2016, 2017; Crockford et al., 2017), no systematic iron speciation and total organic carbon (TOC) studies were conducted in the Bambuí Basin stratigraphy.

Thus, to understand the paleoenvironmental evolution of a partially isolated Neoproterozoic marine system, we investigated carbonate and shale successions from the Neoproterozoic Carrancas Formation and Bambuí Group (Bambuí Basin) through the analysis of Iron speciation, TOC, provenance (Chemical index of alteration from Nesbitt & Young, 1982 + source evaluation), RSE enrichments, rare earth and trace element variations and 13C and 18O analyses. Our data shows that evolution of this partially isolated intracratonic basin leads to major changes in the seawater redox structure and on the RSE reservoir. The lack of connection with an open marine source also drastically changed the re-supply of marine inorganic input thus influencing bioproductivity and biological activity.

2.2) Geological Background

The Bambuí basin covers the majority of the São Francisco craton in eastern Brazil, exposing a large diversity of Neoproterozoic terrigenous-carbonatic mixed deposits (fig. 2.1). Those record paleoecological episodes of glaciation, subsequent ice melting and eustatic sea level forming an intracratonic basin, which is ecologically associated with the rising of oxygen levels and the origin of early Ediacaran Fauna on West Gondwana (Vieira et al., 2007; Alkmim & Martins-Neto, 2012; Caxito et al., 2012, 2018; Warren et al., 2014). The base of the Bambuí basin stratigraphy is marked by glaciogenic sedimentary rocks, which includes diamictites, associated shales, sandstones and local striated pavements of the Jequitai Formation (Isotta et al., 1969; Karfunkel et al., 2002; Cukrov et al. 2005; Chaves et al. 2010; Uhlein et al., 2011). The Carrancas Formation, an unit deposited in localized basement throughs in the southern portion of the basin, has been interpreted as glaciogenic by some authors and correlated to the Jequitaí Formation (Costa and Branco, 1961; Martins-Neto et al., 2001; Reis and Alkmim, 2015). However, Uhlein et al. (2012, 2016), based on stratigraphic and chemostratigraphic proxies, suggest that the sedimentation of the Carrancas Formation was rather controlled by gravitational processes during an episode of minor continental rifting, prior to widespread glaciogenic deposits of the Jequitaí Formation.

Atop the glaciogenic sedimentary rocks and the localized Carrancas Formation, the Bambuí Group is composed of large-scale stratigraphic alternations between carbonatic and siliciclastic successions, which can be grouped into three shallowing-upward megacycles disposed into a shallowing-upward general trend (Martins-Neto, 2009; Alkmim & Martins-Neto 2012; Bertoni et al., 2014; fig 2.2). The deposition of this group is widely debated in the literature, and current models suggest that the Bambuí Group was formed in an intracratonic epicontinental setting (Martins-Neto and Alkmim 2001; Martins & Lemos, 2007) limited by the Brasilia Belt at west, the Araçuai belt to the east, and the Ribeira and Rio Preto belts to south and north respectively (Dardenne et al., 2000; Alkmim & Martins-Neto, 2001, 2012)(fig. 2.1) . In addition, some authors suggest that despite its intracratonic nature, the Bambuí Group stratigraphic record represents a full foreland cycle (Uhlein et al., 2017). It is also suggested that the development of Lower and Upper stratigraphic portions of Bambuí basin took place in isolated epicontinental environments (Vieira et al., 2007; Paula-Santos et al., 2015; Kuchenbecker et al., 2016), following discordant $^{87}Sr/^{86}Sr$ and $\delta 1^{3}C$ signatures (Caxito et al., 2012; Paula-Santos et al., 2014), low abundance of Ediacaran fauna (Warren et al., 2014), while the middle portion of the Basin (e.g. Upper Sete Lagoas Formation) may have experienced limited environmental connection with outer open marine settings (Warren et al., 2014; Paula Santos et al., 2015).

The age of the Bambuí Group is also a matter of intense debate in the recent literature (fig. 2.2). Composing the base of the group, the Sete Lagoas Formation is widely recognized as a typical post-glacial deposit, bearing pinkish cap dolomite featuring a δ13C negative excursion, prominent aragonite fans and barite layers(Vieira et al., 2007; Caxito et al., 2012; Alvarenga et al., 2014; Crockford et al., 2018; Okubo et al., 2018) (fig. 2.2). Babinski et al. (2007) obtained a Pb-Pb isochron age of 740 ± 22 Ma on cap carbonates of this lowermost section, but Babinski et al. (1999), D'Agrella-Filho et al. (2000) and Misi et al., (2005) suggested that Pb-Pb ages might be disrupted by isotopic Pb input from hydrothermal events. Alternatively, Caxito et al. (2012) suggested that the basal Sete lagoas Formation represents a typical post-Marinoan cap carbonate based on the presence of a basal cap dolostone preserving decreasing-upwards negative $\delta^{13}C$ and $\delta^{18}O$ and $^{87}Sr/^{86}Sr$ signatures of 0.7074–0.7076. Recently, new U-Pb ages from detrital zircons were obtained from the middle and upper Sete Lagoas Formation. Paula Santos et al. (2015) obtained a minimum depositional age of 557 Ma from the youngest detrital zircon U-Pb age peak, while Pimentel et al. (2011) acquired minimum depositional ages ranging from 620-610 Ma.

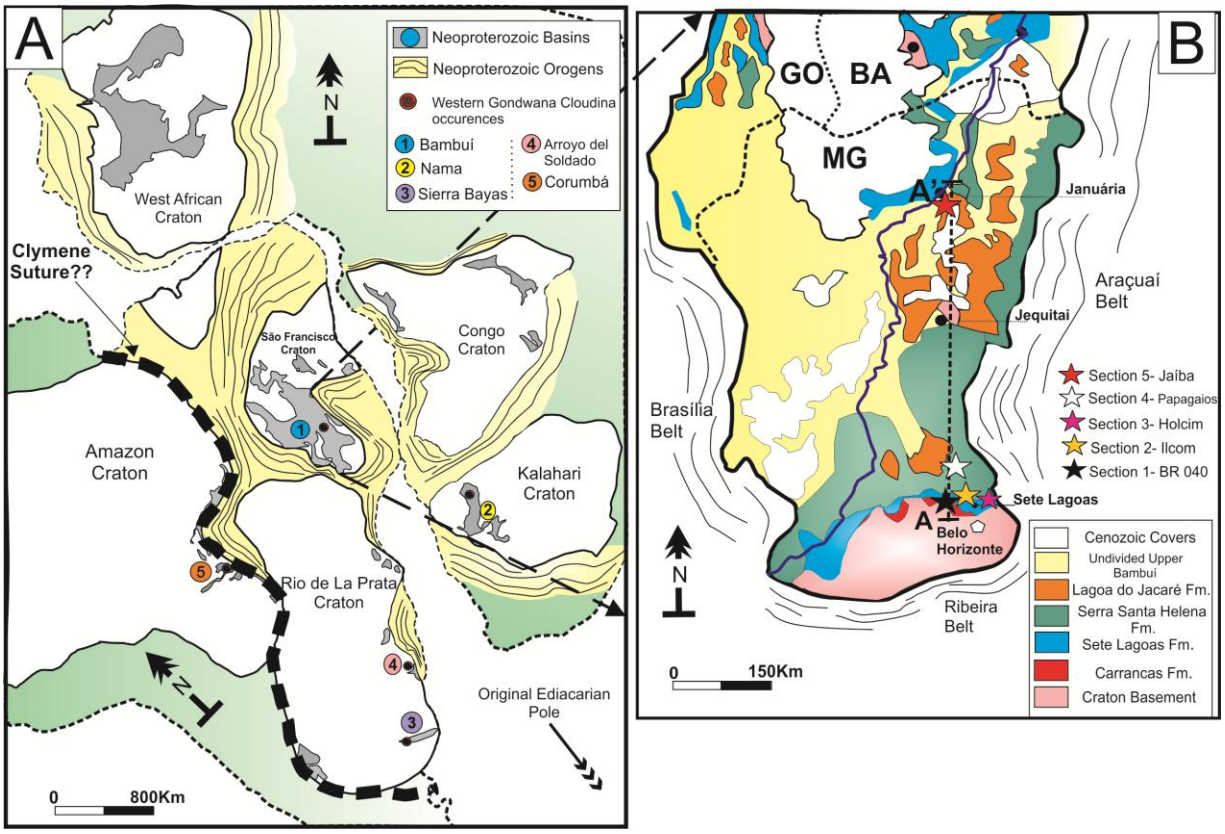

Fig 2.1. A) Ediacaran paleogeographical and tectonic context of the São Francisco Craton on southwest Gondwana, based on modern day continent configuration. After Misi et al. 2005 and Alkmim et al. 2006. B) Local geological context and localization of studied areas. C) Regional cross section showing São Francisco craton basement structure, filled by Bambuí basin deposits (not to scale).

The basal portion of the Sete Lagoas Formation is also marked by lithotypes such as shales, carbonates and pinkish dolomites, which gradually coarse into oolitic and stromatolitic carbonate deposits with subaerial exposition levels at the top of the unit (Dardenne et al., 2000; Vieira et al., 2007; Paula-Santos et al. 2015)(fig. 2.2). According to Vieira (2007) the deposition of the Sete Lagoas Formation was controlled by two main sedimentary settings. The first is responsible for the deposition of the lower portion of the Sete Lagoas Formation and includes deep, low energy deposits formed in a restricted and disconnected marine environment. This environment is controlled by an anoxic/oxic chemocline which yields the concentration and deposition of $CaCO_3$ saturated alkaline deposits including aragonite fans, and ^{56}Fe rich micritic carbonates with strong variations on Ce and other trace element anomalies, followed by the presence of interstitial pyrite and pyrrhotite crystals (Vieira, 2007). The second cycle is responsible for the deposition of the middle and upper Sete Lagoas Formation, represented by open marine, inner ramp high energetic deposits. This deposition is strongly controlled by storm and wave interactions and is also regulated

by riverine detrital input in the form of interbedded marls. Chemically, the middle portion is marked by $\delta^{13}C$ signal stabilization close to 0‰ and the absence of trace element anomalies (Kuchenbecker et al., 2016). The upper section registers a strong $\delta^{13}C$ increase to values up to 10‰ combined with the presence of organic matter-rich stromatolites related to an episode of high carbon burial rate (Vieira et al., 2007).

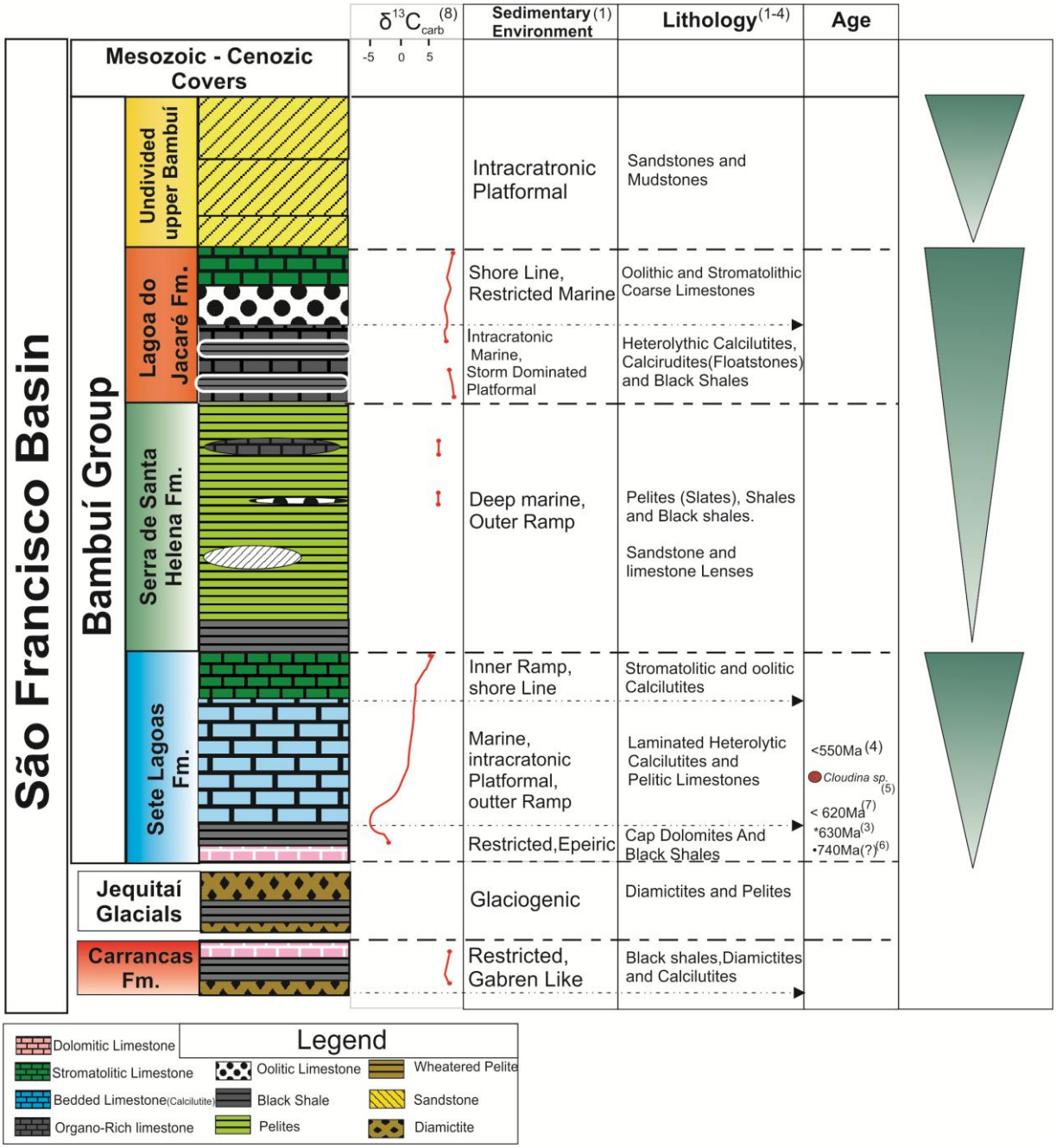

Fig 2.2. Regional stratigraphic chart of São Francisco basin. Refs. - (1) Reis and Suss, 2016; (2) Vieira et al., 2007; (3) Caxito et al., 2012; (4) Paula Santos et al., 2014; (5) Warren et al., 2014; (6) Babinski et al., 2007; (7) Pimentel et al., 2012; (8) Reis, 2013.

Overlying the Sete Lagoas Formation, the second coarsening-upward megacycle is represented by the Serra de Santa Helena and Lagoa do Jacaré formations (Alkmim & Martins-Neto, 2001, 2012) (fig. 2.2). The Serra de Santa Helena Formation is mainly represented by greenish shales with local presence of pyrite, which can be locally alternated by thin sandstone levels. Platformal structures such as storm-related cross stratifications and symmetric ripple marks are also observable on sandstones. At the top of the unit, close to the transition to the Lagoa do Jacaré Formation, coarse-grained lenses of oolithic carbonates can be locally observed yielding strong positive $\delta^{13}C$ signals ranging from 6.0 to 8.0‰, marking a transition to a shallower depositional environment (Reis, 2013)(fig. 2.2).

These platform deposits gradually give place to shallow, highly energetic shoreline and mid platformal carbonatic deposits of the Lagoa do Jacaré Formation. This interval is represented by dark carbonates that gradually shifts from fine-grained parallel laminated platformal carbonates, to shoreline coarse-grained oolithic lenses with wavy and cross stratification structures at the top of the formation (Reis, 2013). The succession also includes lithotypes such as marls with storm-related structures, black shale lenses, siltites and local dolomites. Following the chemostratigraphic trend of the carbonatic lenses of the Serra de Santa Helena formation, carbonatic rocks from the Lagoa do Jacaré Formation exhibit strong positive values of $\delta^{13}C$ ranging from 8 to 13‰ (Reis, 2013) (fig. 2.2).

The last coarsening upward cycle of the Bambuí Group, represented by the Serra da Saudade and Três Marias formations (Alkmim & Martins-Neto, 2001, 2012) is informally nominated as undivided upper Bambuí in this work. This unit is essentially composed of clastic marine to alluvial sediments (fig. 2.2).

2.3) Material and Methods

2.3.1 Stratigraphic sections

To constrain the biogeochemical evolution of the Bambuí basin, five stratigraphic sections covering from the Carrancas to the Lagoa do Jacaré formations were selected (fig. 2.3) according to the presence of key stratigraphic features. Among these features, the presence of black shale intercalations, the presence of pyrite framboids and aggregates, organic matter preservation, and the whole of representativeness of the Bambuí basin stratigraphic framework were accounted to select the following stratigraphic sections analyzed in this paper (figs. 2.3 and 2.4).

2.3.2 Major and Trace elements geochemistry

Trace and Rare Earth element analysis were carried in a Quadrupole Inductively Coupled Plasma Mass Spectrometer Q-ICP-MS (Agillent 7700x) and Major elements were analyzed in an Agillent 725 Inductively Coupled Plasma Optical Emission Spectrometer (ICP-OES) at the Geochemistry Laboratory (LGqA) at Universidade Federal de Ouro Preto (UFOP). Analytical precision was generally better than 5% and detection limits are below 0.01 ppm for rare earth and trace elements and below 2 ppm for major elements. Acid digestion and table-top procedures followed the steps described by Magela & Enzweiler (2015), which optimize acid dissolution methodology in order to improve REE recovery from iron rich sediments.

To access the role of major element enrichment or depletions relative to a typical detrital average, calculations of element enrichment factors are commonplace (Tribovillard et al., 2006). Due to its immobile character Al is used to normalize major elements abundances, and then divided by a known detrital source ratio such as the Post Australian Archean Shale (PAAS) from Taylor and McLennan (1985). Following Tribovillard et al. (2006) a given major element enrichment factor (MEF) can be calculate by: MEF=((MESample /AlSample)/(MEPAAS/AlPAAS)). To address major elements variability on carbonate samples, results were compared with the carbonate average from Turkhein & Wedphol (1962).

To access the role of authigenic trace element enrichment and dilute element total abundance, normalization against elements such as Al, Th, Sc, Ti, Zr and Cr are usual (Brumsack, 2006; Tribovillard, 2006). Besides their immobile character during diagenesis and post depositional process, these elements are also concentrated on the detrital fraction of sediments and can be used as a tracer for detrital input (Brumsack, 2006; Tribovillard, 2006). Among these elements, Al trace element normalizations are widely used, though some drawbacks may be related to post depositional, surface weathering enrichments on sediments exposed to tropical climate (Van der Weijden, 2002). In fact, Kuchenbecker et al. (2016) observed large disturbances on major and trace element content from Sete Lagoas Formation carbonates related to secondary processes. To avoid Al overconcentration and access a lithology independent detrital input tracer, Th has been successfully used on mixed (shale-carbonate) successions as a normalization proxy (Schroder and Grotzinger, 2007) even to sediments exposed to strong surface weathering (e.g Corumbá Group; Spangenberg et al., 2014). In order to check Th secondary enrichments or loss and to confirm its detrital nature, cross plots against other detrital elements (Cr, Zr) are suggested (Tribovillard, 2006). In our samples, strong correlations between Th and Cr (R^2 =0.94, n=35) and Th and Zr (R^2 =0.97, n=35) attests Th as good normalization tracer (See supplementary material).

To avoid lithology-related enrichment masking, TE/Th ratios were compared against two different standards for sediments deposited in oxic conditions. As usual, TE/Th ratios for shale samples were compared with PAAS values from Taylor and McLennan (1985), and following Schroder and Grotzinger (2007) and Spangenberg et al. (2014) all carbonatic rocks were compared to average crustal carbonatic rocks values from Turekian and Wedepohl (1961). For comparison purposes, enrichment factors were calculated following Tribovillard (2006) on which Trace element (TE) enrichment factor (EF) is given by SEF= $(TEx/Th)_{sample}/(TEx/Th)_{PAAS}$ for shales and CEF= $(TEx/Th)_{sample}/(TEx/Th)_{Average\ carbonate}$ for limestones.

2.3.3 Rare earth elements

Rare earth elements (REE) values were normalized (XPN) against Post Archean Australian Shale (PAAS) from Taylor and McLennan, (1985). Avoiding La normalizations due to overconcentration of La on seawater (Lawrence et al., 2006), Eu and Ce anomalies were calculated following Lawrence and Kamber (2006), where Eu/Eu*= EuPN(SmPN2*TbPN)1/3 and Ce/Ce*= CePN/(PrPN2/NdPN). Light rare earth element (LREE) and Medium rare earth element (MREE) enrichments were calculated according to Frimmel, 2009: LREE= (Sm/Yb)PN and MREE=(Tb/[(Nd + Tm)/2]PN).

2.3.4 Chemical index of alteration(CIA) calculations and provenance plots

Following Kronberg et al. (1986), CaO contents are generally fixed to NaO, as in most siliciclastic rocks NaO contents are associated to the detrital fraction and present low variance. Unlikely, the studied samples show a wide range of NaO contents (S^2=0,27) which invalidates NaO as a CaO fixer. To solve this issue, CaO contents were fixed to TiO contents as nearly all of Ti is linked to detrital phases (Roser and Korsch, 1988), and the element presents very low variance (S^2=0,01) in our samples. A limiting CaO/TiO ratio of 1,3 from PAAS was used to fix CaO contents, as PAAS is widely used as a standard for CIA studies (Fedo et al., 1995; Kunzmann et al., 2015). Ternary plots with major element abundances were plotted together with local contemporaneous igneous rocks (gabbroic plutonic from Novo, 2009 and felsic volcanic rocks from Vieira, 2007), besides PAAS and Upper continental crust (UCC) to analyze source chemic variability. Selected source rock evaluation plots Tio_2/Al_2O_3 vs La/Yb, Tio2 vs Zr (Hayashi et al., 1997), and La/Th vs Hf (Floyd and Leveridge, 1987) were plotted together with Contemporaneous arc related igneous rocks, PAAS and Upper continental crust (UCC) values for comparison purposes.

2.3.5 Iron speciation

One sample from each studied stratigraphic section was selected for iron speciation methodology. The five step sequential extraction scheme from Poulton and Canfield (2005) was followed in order to separate FeCarb, FeOx, and Fe Mag pools. FePy was extracted from a different sample aliquot following the digestion scheme proposed by Lord III (1982). As shown by Huerta-Diaz and Morse (1990), this FePy extraction scheme yield similar FePy concentrations (R2=0.92; n=50) relatively to the Cr-reduction scheme from Canfield et al. (1986), showing that both methodologies quantitatively accessed almost all available Fe from pyrite. All Fe pools (FeCarb, FeOx, Fe Mag and FePy) were analyzed in an ICP-OES (Agillent 725), as ICP-OES yield comparatively better results than other analytical methods (Kunzmann et al., 2015). Duplicates samples yield reproducibility better than 5 %.

2.3.6 Total Organic Carbon (TOC)

Total organic carbon analysis were carried in the GSG-Geosol lab. Samples were analyzed by Combustion Infrared Detection Technique in a LECO model CS-775. Reproducibility on the Standard BXGO-1 was better than 5% and duplicate samples yield reproducibility better than 10%.

2.3.7 Carbon and Oxygen analysis

Carbonates samples were collected for whole rock analyses. The samples were cleaned, cut and powdered. Isotope analyses were carried out at the Laboratory NEG-LABISE of the Federal University of Pernambuco. 20 mg of powdered sample were treated with H3PO4 (100%) in a vacuum at 25°C for the determination of carbon and oxygen isotopes and the resulted CO2 gas analyzed according to the method described by Craig (1957). CO2 gas released by this method was analyzed in a Thermo Finnigan Delta V Advantage mass spectrometer. The external precision based on multiple standard measurements of NBS-19, NBS-18 and NBS-20 was better than 0.1 ‰ versus V-PDB for carbon and oxygen. The results are expressed in the δ notation in parts per thousand (‰) in relation to the international V-PDB scale.

2.4) Results

2.4.1 Stratigraphic Sections

Section 1 - Carrancas Formation, BR 040 (lat/long: -19.624328, -44.205778)

The stratigraphic lowermost section sampled is located on the BR-040 road (figs. 2.1b and 2.4a) between the cities of Belo Horizonte and Sete Lagoas at the central portion of the Minas

Gerais State. The section comprises up to 40 m of the Carrancas Formation which onlaps the São Francisco craton basement in a typical gabren-like deposit at the base and is overlain sharply by Sete Lagoas Formation laminated limestones at the top (fig. 2.3). The section is constituted by dominant gray mudstones alternated by decametric packs of fine laminated black shales and minor decimetric layers of diamictite. Ferruginous siltstones and associated Fe-Mn oxide segregations are also interbedded within black shale layers. These features are generally followed by strong outcrop scale weathering, transforming dark black shales into yellowish mudstones. Five fresh and visually clean samples were taken from the black shale intervals, and to constrain the whole of weathering and post-depositional alteration, two samples were taken from weathered black shale levels for comparison purposes (fig. 2.3).

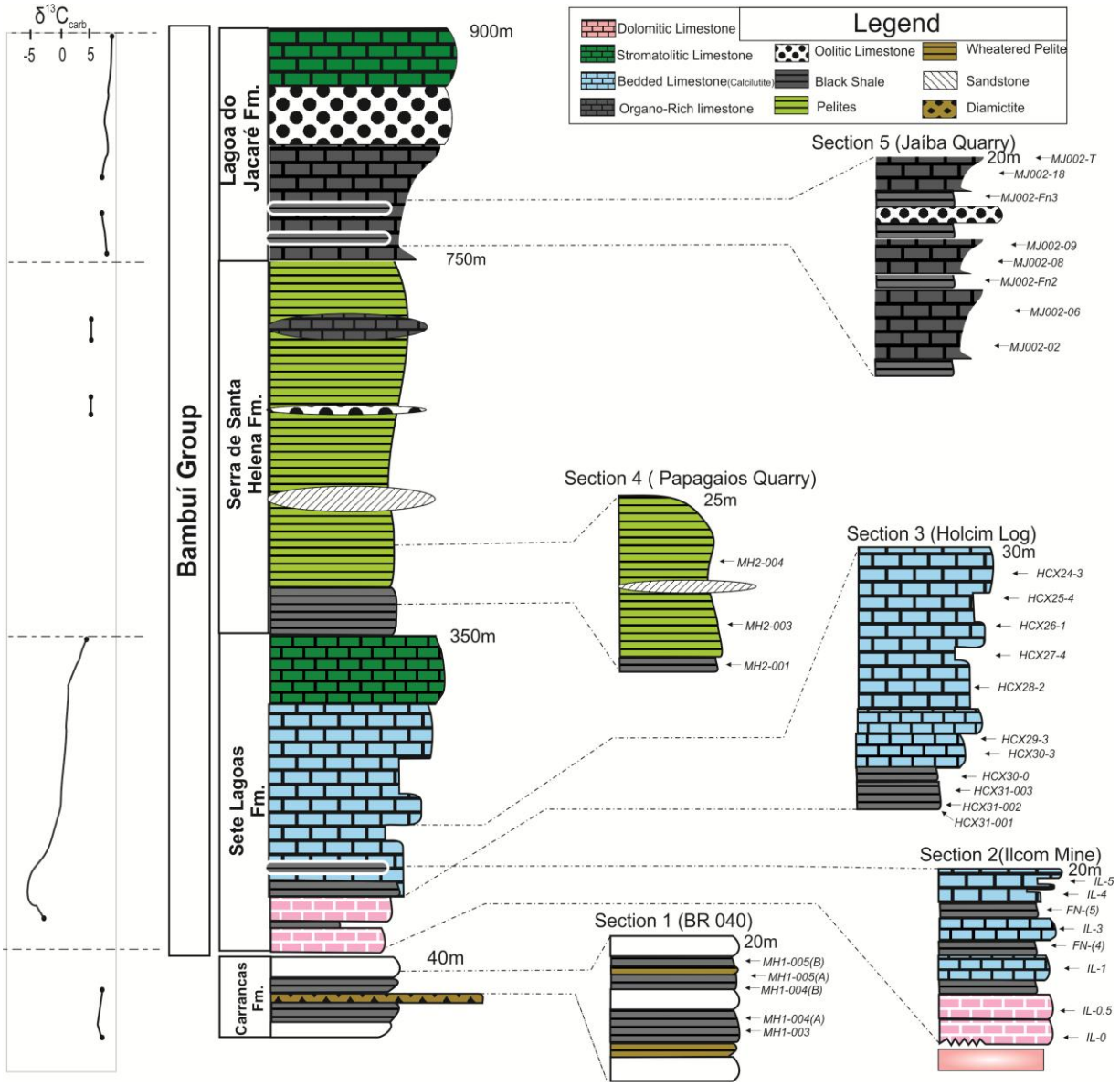

Fig 2.3. Stratigraphic placement of studied sections in the Bambui Basin column. All of the 35 samples analyzed for trace and REE geochemistry are shown in stratigraphic height on each local section. Regional Bambuí column was based on Reis & Suss, 2016. $\delta^{13}C$ data is from Reis, 2013.

Section 2 - Ilcom Quarry - Sete Lagoas (lat/long: -19.493029,-44.258050)

Section 2 is located near the city of Sete Lagoas, in a quarry named Ilcom (figs. 2.1b,2.4b). The profile is marked by the prominent exposure of the São Francisco craton basement in direct contact with onlapping dolomites and limestones of the Sete Lagoas Formation. Sampling was gently allowed by Ilcom Mineração Indústria e Comércio Ltda.

At the contact, a 1.5 m thick layer of whitish fine-grained dolomite onlaps the basement. These dolomites are gradually overlain by a second 1.5 m thick fine-grained pink dolomitic limestone. In a sharp contact, these limestones are followed by a 20 cm-thick layer of black shale which in turn is overlaid by 0.5 m thick layer of thin laminated heterolythic calcilutites. The section is followed by a 6 m thick interval of laminated calcilutites intercalated to 10-20 cm-thick black shale layers. Five limestone specimens and two black shale layers were sampled in total (fig. 2.3).

Section 3 - Holcim Mine drillcore, Pedro Leopoldo (lat/long: -19.605223, -44.059066))

The third section analyzed in this study encompasses the lower portion of the Sete Lagoas Formation. The Log was drilled 180 m deep at the Holcim Mine site, in the city of Pedro Leopoldo. Sampling of the drillcore was gently allowed by Holcim Brasil S.A. (fig. 2.1b).

The Log section comprises up to 30 m of alternated layers of grey-greenish heterolythic bedded calcilutites and basal black shales (fig. 2.3). The section begins with a 5 m thick layer of bright dark black shales. These black shales are overlain by a massive 30 m thick succession of fine-medium grained calcilutites. Most of this upper succession is constituted by centimeter-thick heterolythic bedded layers of alternating fine and medium grained calcilutites. Rarely, centimetric lenses of black shale are also observed through the log. Four black shale and seven limestone samples were taken for trace and REE element analysis.

Section 4 - Papagaios Quarry (lat/long: -19.35241,-44.775167)

At the vicinities of the city of Papagaios (fig. 2.1b), the quarry is a nearly 80 m deep pit exposing the lower portion of the Serra de Santa Helena Formation. The quarry is marked by strong lithologic and stratigraphic homogeneity, where the 40 m of the exposed section is mainly

represented by thin laminated, flat lying dark greenish shale of the Serra de Santa Helena Formation (fig. 2.4c).

Isolated layers of pyrite-rich shale are observable at the base of the section. These specimens are generally represented by shales with darker colors and thinner laminations. The pyrite aggregates in these rocks are randomly disseminated through the host in single, well formed very fine grains. Two other pyrite-free samples were taken for comparative purposes.

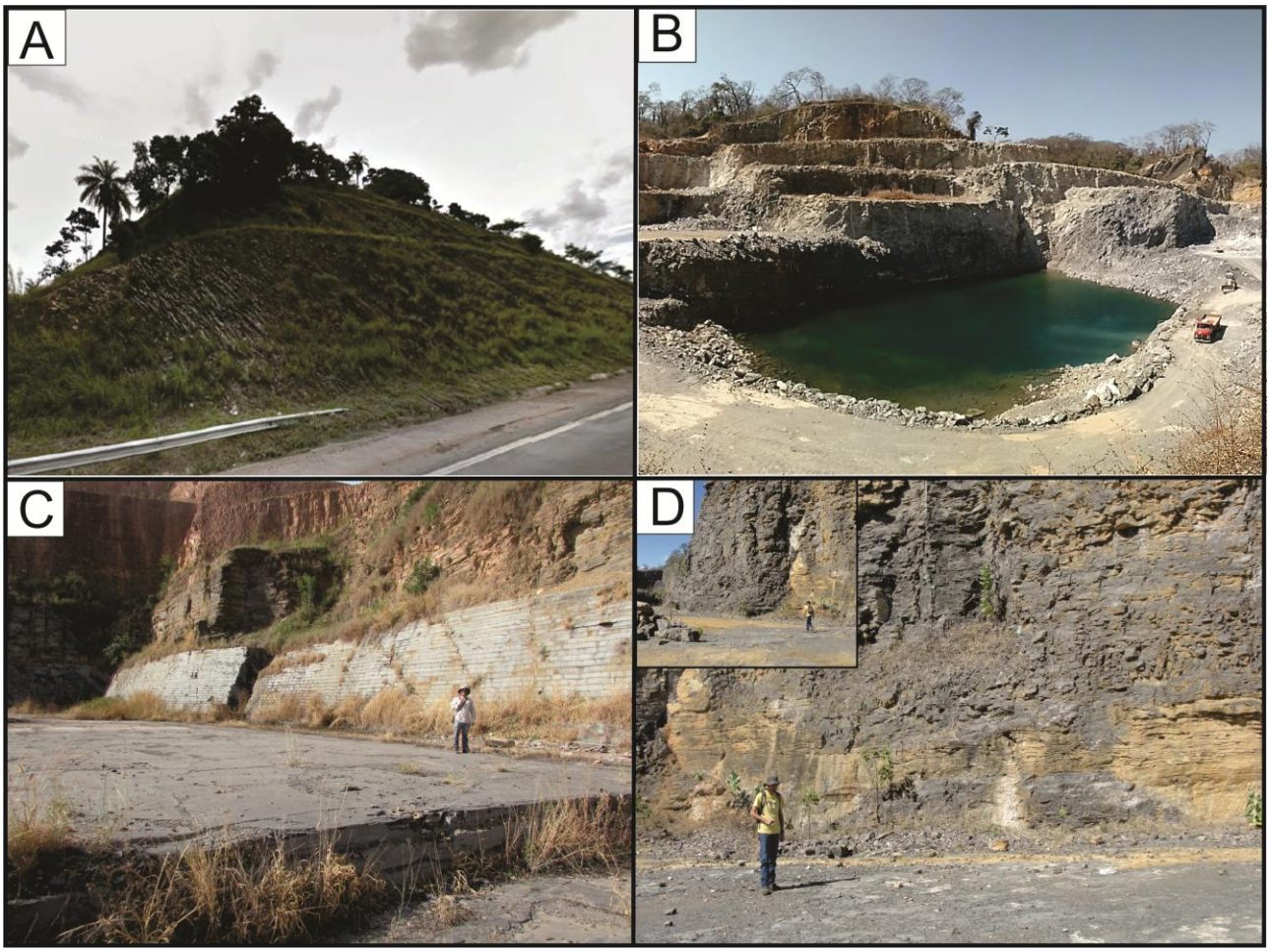

Fig 2.4. Broad view of studied sections. A) Carrancas section (1) located in a road (BR-040) outcrop Between Belo Horizonte and Sete Lagoas. B) Section 2 (Lower Sete lagoas Fm.), located at the Ilcom Quarry near Sete Lagoas. Truck at the right portion of the picture for scale. C) Section 4 (Serra de Santa Helena Fm.) at Papagaios quarry located in the city of Papagaios. D) Two different broad views (upper corner) from section 5 (Lagoa do Jacare Fm.), located at Jaíba.

Section 5 - Lagoa do Jacaré Formation, Jaíba (lat/long: -15.12395, -43.54266)

Cropping out in the central portion of the Bambuí basin, the 5th section is located close to the city of Jaíba (Northen Minas Gerais state). This section comprises the lower portion of Lagoa do Jacaré Formation that was sampled from a small abandoned quarry.

The section comprises up to 25m of alternated dark carbonatic rocks and associated black shale layers (fig. 2.4d). All the limestone specimens show diagnostic features of storm-related platformal deposits in the lower portion of the profile. Coarse calcirudites are abundant presenting undulated beds and large calcilutite clasts. The section is also followed by calcirudites with hummocky structures and calcilutites with heterolythic bedding featuring wavy and linsen structures. Some of the calcirudites can also be oolithic and tend to be associated with fining upward beds. Black shale layers are also interbedded between the rock types, forming decimetric continuous layers, with reasonable lateral continuity.

Limestone specimens were taken according to its representativeness from the stratigraphic and lithological variability of the section, totalizing six samples. A total of two black shale samples were taken from individual and distinct layers of the profile (fig. 2.3).

2.4.2. Provenance data

CIA numeric results are in figure 2.5, and major element data are displayed on ternary plots from figure 2.6. CIA highest values are found on Carrancas Fm. samples (Average = 78). It decreases to 70 on Sete Lagoas Fm. samples and to a minimum of 69 on Serra de Santa Helena and Lagoa do Jacaré Fm. This decrease on CIA values from Carrancas Fm. is associated with decreases on Al (mean 15% wt) contents and increase on Mg (mean = 5.7% wt; MEF=3.26), Ca (mean = 2.68% wt; MEF=2,77), K (mean = 5.22% wt; MEF=1.78) and Fe (mean = 5.5 %; MEF=0.96) on Sete Lagoas Formation. The same trend is observed on Serra de Santa Helena and Lagoa do Jacaré formations samples where Al concentrations ranges from 14-7% wt; Ca presents the greatest enrichments (mean = 4.5% ; MEF= 6.6), followed by Mg (mean = 3.77%; MEF = 3.11), Fe (mean = 7.7%; MEF =1.75, K (mean = 3.0%; MEF=1.46), Na (mean = 1.1%; MEF= 1.31) and Mn (mean = 707 ppm; MEF = 1.2). Strong covariations of these major elements are observed on Carrancas Fm. samples where K and Na are strongly covariant (R2 = 0.9) and present strong affinity with Mg (K-Mg R2 = 0.9 and Na-K R2 = 0.8) and also on Serra de Santa Helena de Santa Helena and Lagoa do Jacaré Fm. samples, whereAl presents strong correlations with K (R2=0.99), Na (R2=0.95), and Mn (R2=0.75).

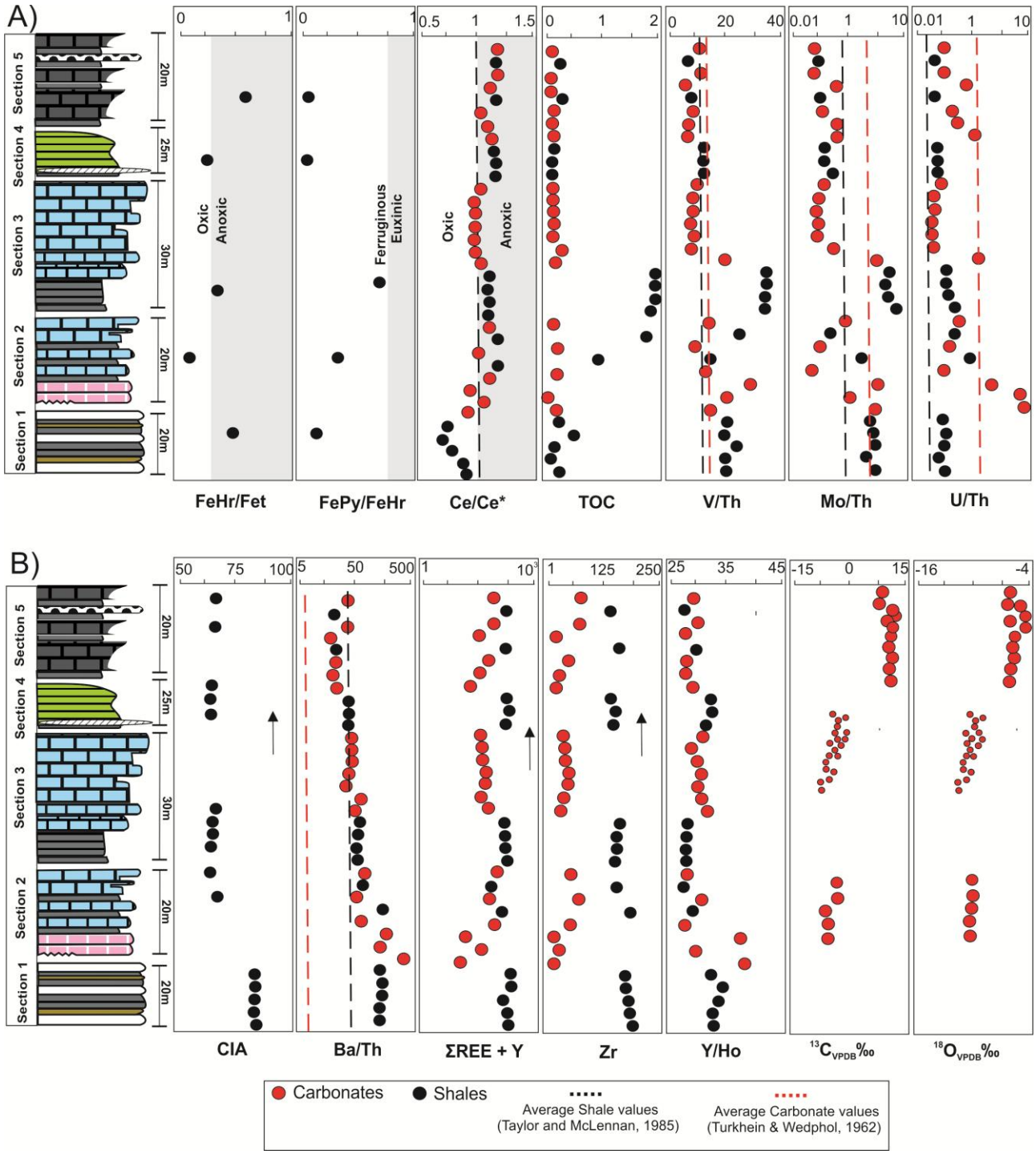

Fig.2.5. A) Redox proxies results from all studied sections. B) Selected REE, Ba and CIA and stable isotope proxies from studied sections. Importantly, stratigraphic sections are in order, though not on stratigraphic continuity.

Provenance data is plotted on figure 2.7. All the selected plots including Tio_2/Al_2O_3 vs La/Yb, Tio_2 vs Zr, and La/Th vs Hf yield comparable results, presenting low chemical variability and no source-related chemical heterogeneities.

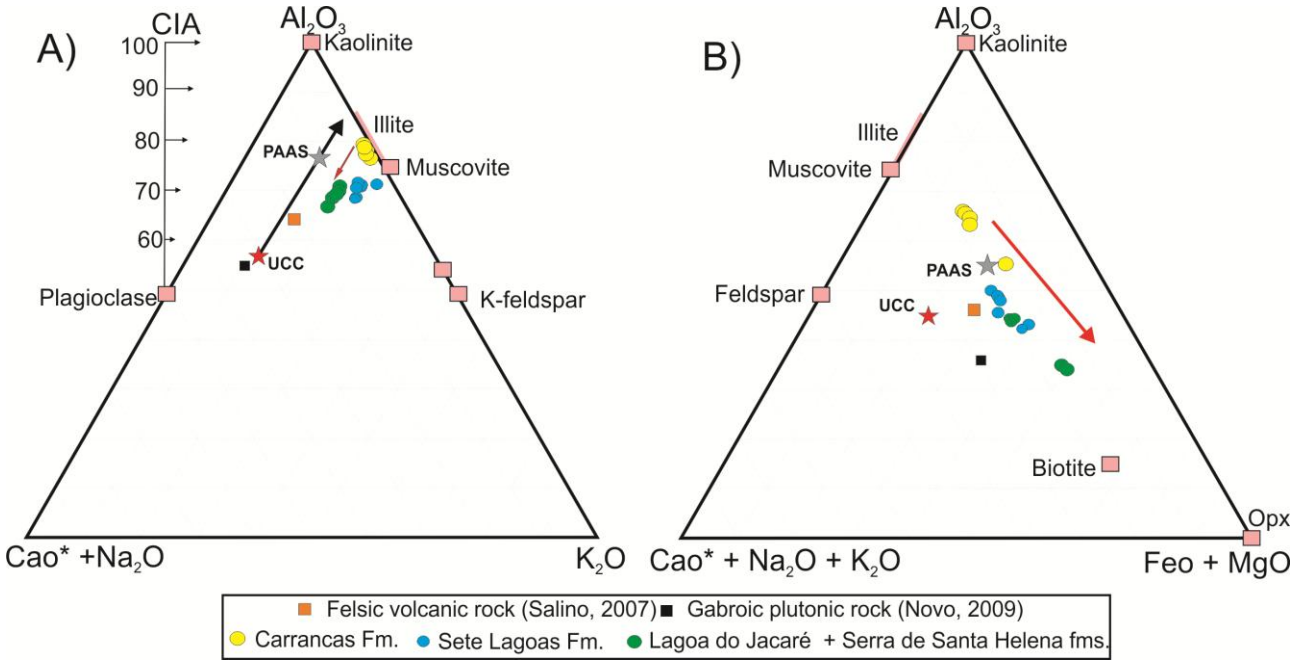

Fig. 2.6. Ternary major elements plots. A) Cao +Na2O-Al2O3+ K2O ternary plots, where the black arrow represent the normal chemical weathering trend from crustal materials (upper continental crust) towards clastic sediments (PAAS) from Taylor and McLennan (1985). Note that conversely, our samples moves from strongly weathered values towards less weathered samples (red arrow). B) Cao +Na_2O-Al_2O_3+ K_2O + FeO+MgO ternary plots. Black marks the chemical transition from Al rich samples (e.g Carrancas Fm.) towards samples with decreased Al contents and higher (Cao +Na2O+ Feo+MgO) (e.g Sete Lagoas, Serra de Santa Helena and Lagoa do Jacaré fms.

2.4.3. RSE, Ba and other Trace element data

Shales

Ba presents the greatest enrichments on shales (figs. 2.5 and 2.8d) with average values of 1297 ppm (n=16; Average Ba/Th =102 and SEF =2.31). Related to Ba, the highest enrichment factors are found on the lower portion of the section comprising Carrancas (SEF=3.7) and Sete Lagoas Fm. (SEF=3.2) while stratigraphically upper samples are generally depleted on Ba. These enrichments are also shown by Ba X Al and Ba X Zr crossplots on shale and carbonate samples where Ba contents of Carrancas and Sete Lagoas formation are above PAAS ratios, while Serra de Santa Helena and Lagoa do Jacaré formations presents Ba X Zr and Ba X Al ratios below PAAS values (fig.2.8d). Co and Cr are slightly enriched in all sections (SEF=1.27) except for Carrancas Formation samples that presents strong depletions (Co_{SEF}=0.139 and Cr_{SEF}=0.95). Redox sensitive elements (RSE) V, Mo, U are strongly enriched and covariates on the Carrancas and Sete Lagoas formations (both sections)(figs. 2.5 and 2.8a,c). The enrichments of RSE decrease upsection on the Serra de Santa Helena and Lagoa do Jacaré Fms., though some covariance is still observable. V is

the most enriched and abundant RSE (average = 220 ppm), with average SEF= 1.94 on Carrancas Formation, 3.25 on Holcim section and 1.87 on Ilcom Section. U and Mo are characterized by generally low contents in all sections, though strong enrichments are verified in Carrancas Formation (Mo_{SEF}= 4.5 and U_{SEF}=1.342) and on Sete Lagoas Formation shales, presenting a total U_{SEF}=2.16 and a Mo_{SEF}=6.17 (fig. 2.8ba,c). Upper units (Serra de Santa Helena and Lagoa do Jacaré fms.) present slightly depleted and no covariant U, Mo and V contents. U, V, Mo, Cu and Zn enrichments presents weak correlations with Zr, indicating an authigenic origin (fig. 2.8a). See appendix for detailed results.

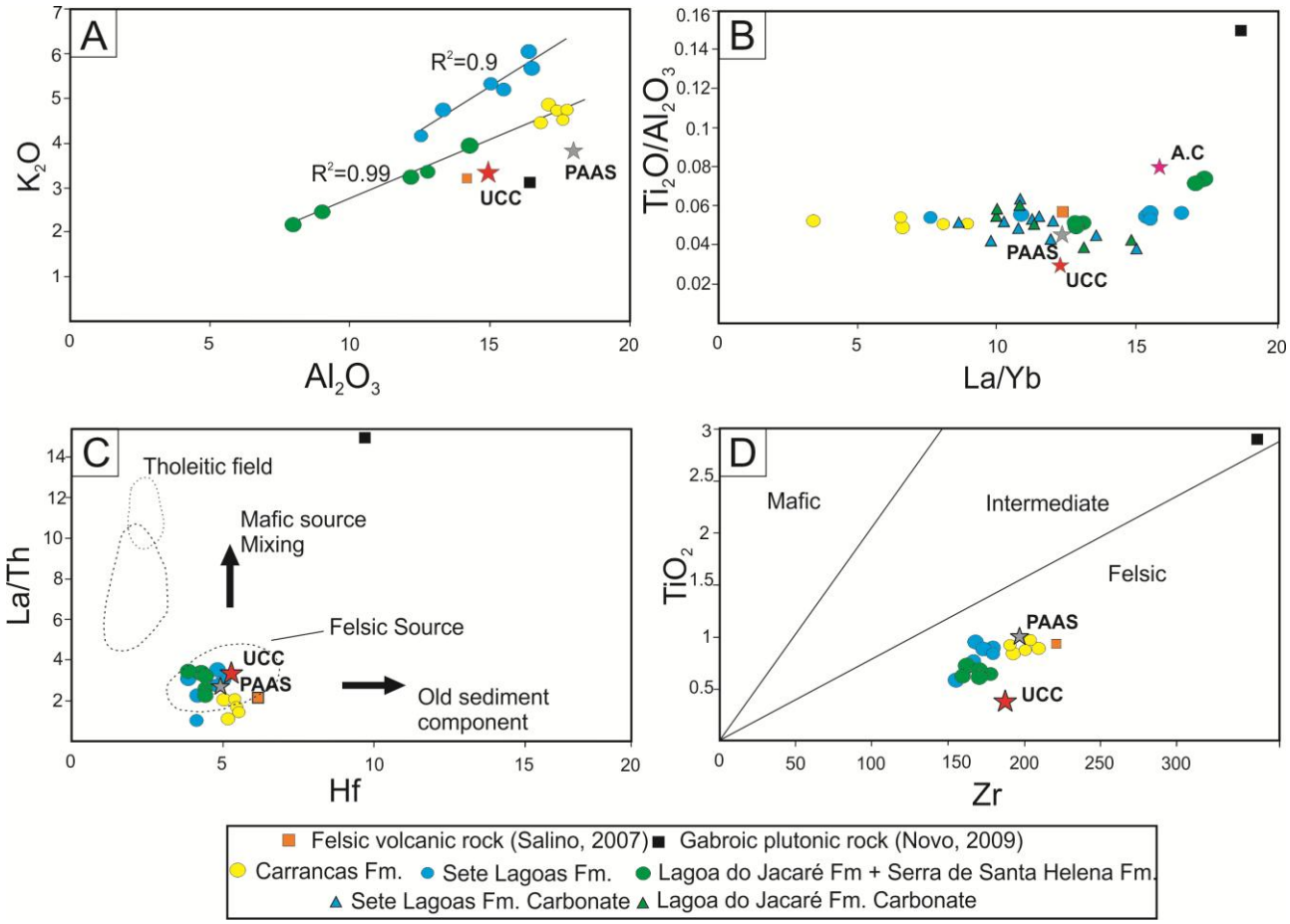

Fig 2.7. Provenance plots showing A) K_2O x Al_2O_3; B) Tio_2/Al_2O_3 x La/Yb; C) La/Th vs Hf source discrimination plots from Floyd and Leveridge (1987). D) TiO2 vs Zr source discrimination plots from Hayashi et al. (1997). Note that all provenance plots show low chemical variability (including carbonate samples on fig 2.7b), and point towards a common felsic igneous source(2.7c,d).

Carbonates

Ba is also enriched on carbonate samples, with average concentrations of 112 ppm (n=19; average Ba/Th=82.2 and total CEF=14.0) This enrichment is specially preserved in the Sete Lagoas Fm. (CEF= 19.2), while samples from Lagoa do Jacaré Fm. section are depleted (fig. 2.8d). Redox sensitive detrital metals Co and Cr are enriched on Ilcom section, though Cr depletion and Co enrichment are observed on Holcim and Jaíba sections. Redox sensitive authigenic metals V, Mo, U are enriched and covariant on the Ilcom section (figs. 2.5 and 2.8b,c) (V Average concentration= 22.2 ppm; V_{CEF}= 1.34, U_{CEF}= 4.32), decreasing upsection towards depletion on Holcim and Jaíba sections (fig. 2.5). V, U and Mo show weak correlation with detrital proxies (Zr) although V and Ni can show some moderate correlation with Zr indicating minor detrital contribution (fig. 2.8b). See supplementary material for detailed results.

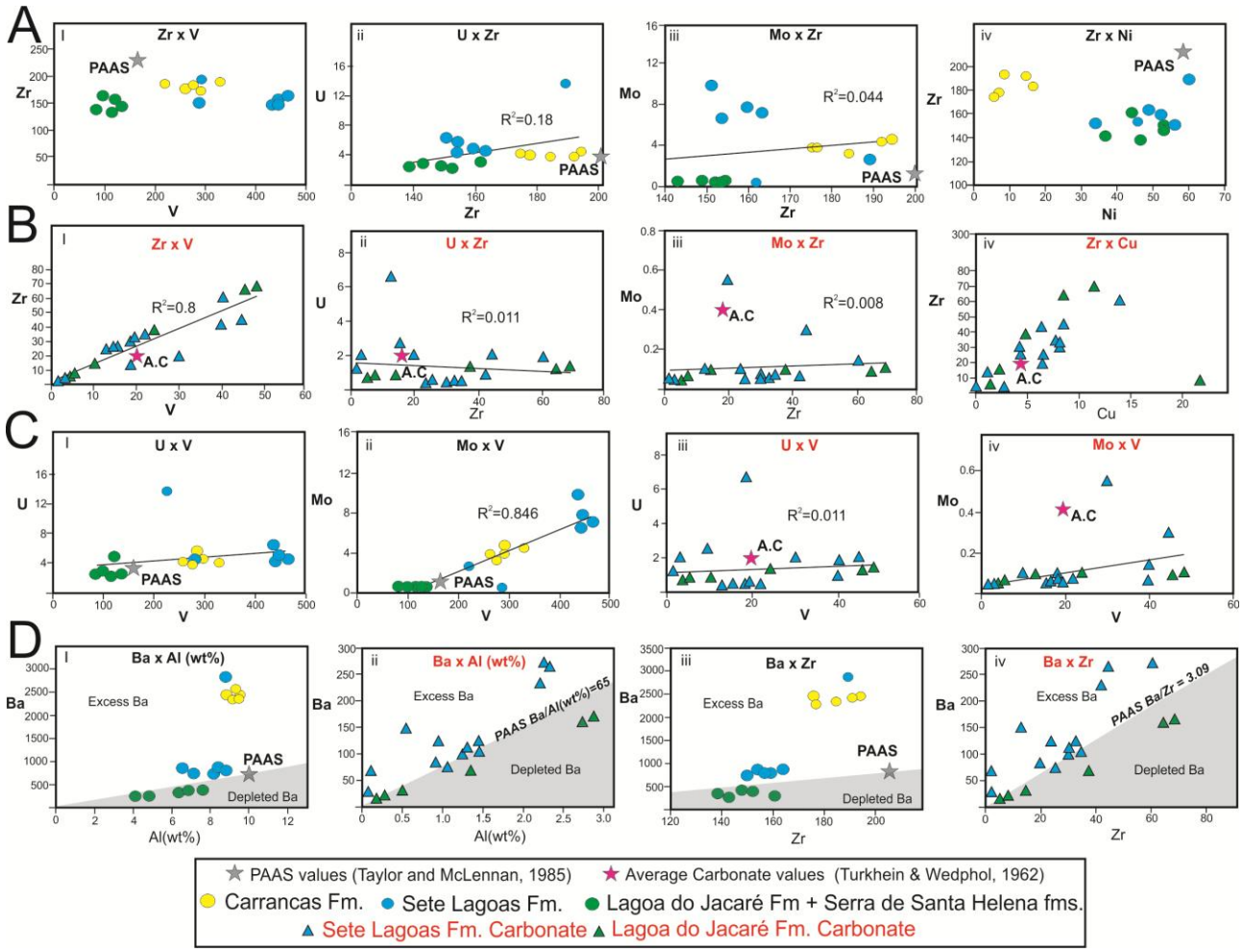

Fig. 2.8. Trace element cross plots (concentrations on ppm) between a) V,U,Mo and Ni X Zr on shale samples indicating low covariance of RSE with detrital elements (Zr) b) V,U,Mo and Cu x Zr on carbonates (Same as item a). c) VxU, VxMo, of shale and carbon showing strong covariations between these elements, suggesting a authigenic origin. D) Ba X Al and Ba x Zr plots of carbonates and shale samples against PAAS detrital average, showing that on both carbonate and shale samples, Sete Lagoas Formation presents enriched (Excess) Ba values, while Lagoa do Jacaré + Serra de Santa Helena fms. presents depleted Ba contents, which can be indicative of enhanced bioproductivity on lower Bambuí Basin stratigraphies.

2.4.4. Rare earth elements

REE distributions on the studied sections can be grouped into three distinct geochemical groups (figs. 2.5 and 2.9). Non-normalized REE data can be found on the appendix section. Ce/Ce* ratios and $\sum \text{REE} + \text{Y}$ abundances are in figure 2.5, and REE (PAAS) normalized plots are in figure 2.9.

The first geochemical group represents the Carrancas Formation and is characterized by REEPN (PAAS-normalized) patterns which strongly resembles open marine deposits, featuring LREE depletion (average LREE=0.74) over MREE (average MREE=1.07) and HREE enrichment (fig. 2.9). Following this open marine trend the group is also marked by relatively high Y anomalies (Average Y/Ho= 32.7) and strongly negative Ce anomalies (Ce/Ce* Average = 0.76). The average $\sum \text{REE} + \text{Y}$ is 224 ppm (slightly above the PAAS value of $\sum \text{REE} + \text{Y}$ =215) and has a strong correlation with Zr (R^2=0.87, not shown).

The second geochemical group encompasses both sections from Sete Lagoas Formation. Unlike group 1, the Sete Lagoas Fm. presents flattened REEPN patterns, with no obvious correlative signature (figs. 2.9 b,c). Shales tend to present flatter patterns with no distinct MREE and HREE enrichment over LREE. Y anomalies are low (Average Y/Ho=26.6) close to crustal values, Ce anomalies are slightly positive (Ce/Ce* average =1.09) and average $\sum \text{REE} + \text{Y}$ is 167.2 ppm (< PAAS concentrations) and no correlation with Zr values are observed (fig. 2.5). On the other hand, carbonate specimens from this second group can be split into pure (no detrital components) and impure carbonates by a threshold value of Zr < 4ppm (Frimmel, 2009). In this scenario, two samples (IL-0 and IL-1) from Ilcom section were classified as pure carbonates. Surprisingly, REEPN patterns from these samples yield no obvious REEPN correlative signatures. Conversely, these samples are marked by a strong HREE depletion relative to MREE (up to 1.28) enrichment, and moderate LREE enrichment. Y/Ho values are higher (38.2 and 37.2 respectively), Ce anomalies are very weak (Ce/Ce* around 0.9), and as expected $\sum \text{REE} + \text{Y}$ contents are very low (8.59 and 12.5 ppm respectively). Impure carbonate samples, on the other hand, are characterized by flattened REEPN patterns, with less developed HREE depletions against MREE (MREE Average= 1.03) and LREE(LREE average=1.11). Y/Ho values (average 29.1) are closer to crustal values, and Ce anomalies are weakly positive (average Ce/Ce* =1.01)(figs 2.5. and 2.9).

$\sum$REE + Y contents are higher (average 52.8 ppm) and presents weak correlation with Zr contents (R^2=0.34).

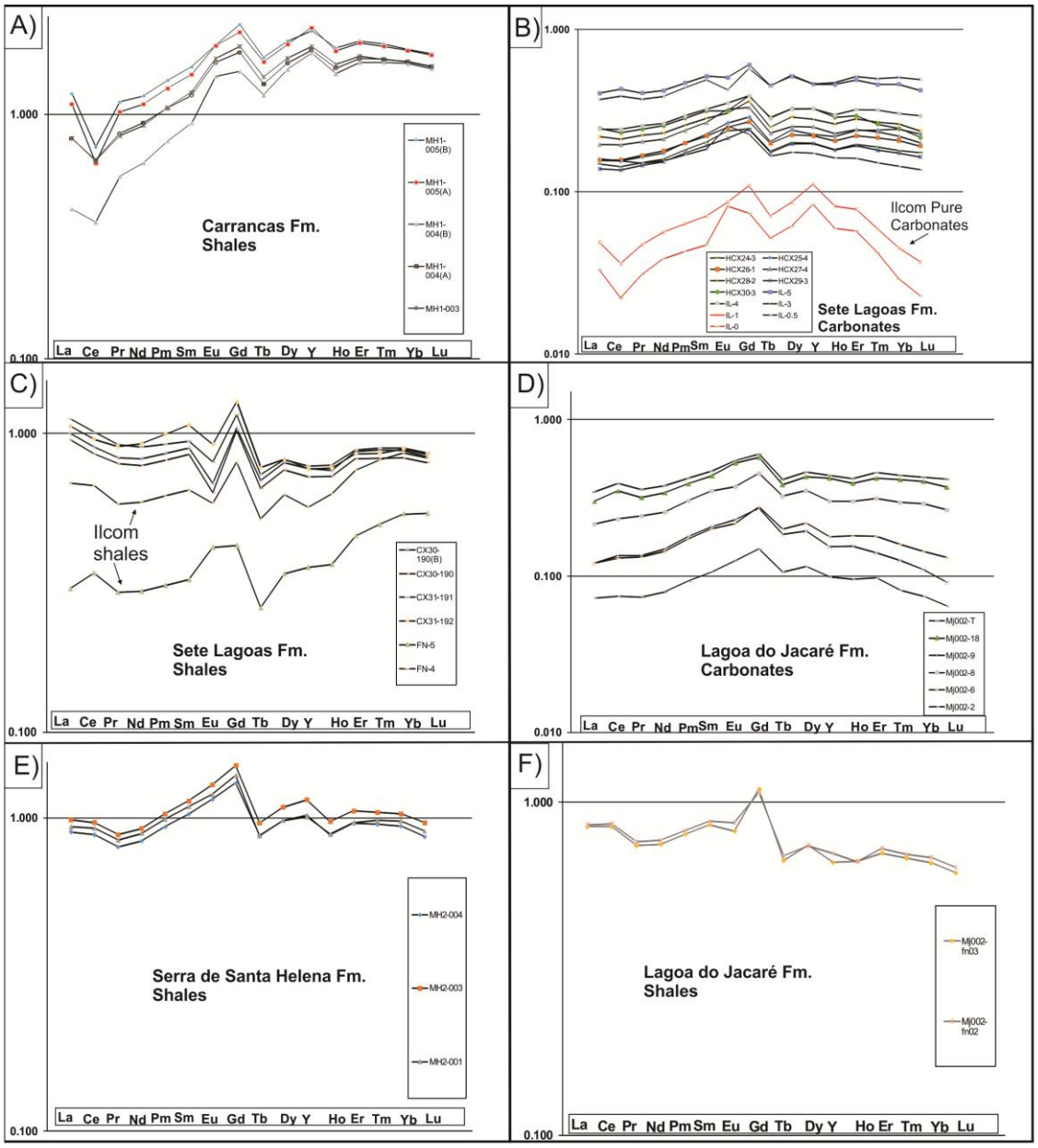

Fig 2.9. PAAS (Taylor and McLennan, 1985) normalized REE plots from A) Carrancas Fm. B) Carbonates from Sete Lagoas Fm. C) Shales from Sete lagoas Fm. D) Carbonates from Lagoa do Jacaré Fm. E) shales from Serra de santa Helena Fm. F) shales from Lagoa do Jacaré Fm..

The third geochemical group comprises Serra de Santa Helena and Lagoa do Jacaré formations. Like group 2, both carbonates and shales from this group features flatten REE/PAAS patterns, with no distinct Gd anomaly (fig. 2.9d,e). Shales are chemically very uniform with almost no HREE depletion over MREE (Average 1.03) and enriched LREE (average = 1.30). Y/Ho values

are low (average =29.7), while Ce anomalies are positive (Average Ce/Ce*=1.14) (figs. 2.5 and 2.9e). $\sum \text{REE} + \text{Y}$ contents are below PAAS (average=166.7 ppm) and a strong correlation with Zr (r^2=0.96) is present. Likely, carbonates from group 3 are also marked by almost no HREE depletion over MREE (average=1.13) and LREE (average = 1.25), though some weak HREE depletion is observed in samples with low $\sum \text{REE} + \text{Y}$ content (e.g MJ002 - 2,6 and 9). Y/Ho values are as low as shale values and Ce anomalies are also positive (average Ce/Ce*=1.1)(figs. 2.5 and 2.9). $\sum \text{REE} + \text{Y}$ contents are high (Average=50.2 ppm)resembling group 2 carbonates and strongly correlated to Zr content (R^2=0.98).

2.4.5. Total Organic Carbon

Total organic carbon values vary between 0.1% up to 2.0% wt (fig. 2.5). The highest values on carbonatic rocks are present on Ilcom samples reaching up to 0.32% on impure samples and below 0.05% on pure samples. Holcim lower carbonate samples yield 0.2%, decreasing up to below 0.05 % on upper samples. Lagoa do Jacaré Fm. samples yield comparably low TOC values between 0.07 and 0.19 % (mean= 0.12%). Shale samples in turn yield higher TOC values averaging 0.4% on Carrancas Fm., 2.0% on Sete Lagoas Fm shales, 0.1% on Serra de Santa Helena and 0.4 % on Lagoa do Jacaré Fm.

2.4.6. Iron speciation

Results of FeHr/Fet and Fepy/FeHr ratios are shown on figure 2.5. Sample MH1-005(A) from Carrancas Fm. yield FeHr/Fet = 0.46 and FePy/FeHr = 0.002 indicating anoxic ferruginous conditions. Sample FN-5 from Ilcom section results were FeHr/Fet = 0.14 and Fepy/FeHr = 0.3 indicating oxic seawater conditions. Sample CX31-192 from Holcim section yield FeHr/Fet = 0.38 and Fepy/FeHr = 0.6 suggesting anoxic ferruginous (almost euxinic) conditions. Serra de Santa Helena Fm. sample MH2-004(A) yield FeHr/Fet =0.37 and Fepy/FeHr = 0.03 indicating dysoxic (almost anoxic) conditions. At last, sample MJ002-FN02 from the Lagoa do Jacaré Formation results were FeHr/Fet = 0.57 and Fepy/FeHr = 0.15 indicating anoxic and ferruginous seawater condition.

2.4.7. $\delta^{13}C$ and $\delta^{18}O$ data

Samples from Ilcom section yield negative $\delta^{13}C$ values ranging from -3.0‰ to -0.4‰. $\delta^{18}O$ values are nearly homogeneous, ranging between -11‰ and -10‰. On the other hand, a extended sample set from Holcim section yield $\delta^{13}C$ values increasing upsection from negative (-3‰) towards weakly positive (0.5‰) values (fig. 2.5b). $\delta^{18}O$ values range between -11‰ and -8‰.

Samples from Lagoa do Jacaré Fm. presents strongly positive $\delta^{13}C$ values averaging 11‰, decreasing to lower values (around 8‰) on upper samples. $\delta^{18}O$ values from Lagoa do Jacaré Fm. samples presents nearly constant values between -6.8‰ and -4.8‰ (fig. 2.5b).

2.5) Discussion

2.5.1. Provenance, detrital input and marine productivity

CIA values range from 79 on Carrancas Fm. Shale, around 70 on Sete Lagoas Fm. shales to a minimum of 68 on Lagoa do Jacaré samples (fig. 2.5b). K_2O-Al_2O_3 plots (fig. 2.7a) show slightly discordant values on Sete Lagoas Fm. shales, exhibiting enriched K values outside the trend line reached between Carrancas, Serra de Santa Helena and Lagoa do Jacaré Fm. (R^2 =0.99). As shown on figure 2.6 (CIA variation and ternary plots), these variations are related to decreases on Al content, which are exchanged with higher Fe, Mg, Ca and Na concentrations on Lagoa do Jacaré and Serra de Santa Helena formations and higher K on Sete Lagoas Fm. samples, in contrast with higher Al on Carrancas Fm. shales. Strong covariation between these major elements on both carbonate and shale samples suggest that these variations are related to the clay mineralogical content of the detrital fraction (Nesbitt and Young, 1982) that shifts from the illite apex on Carrancas and Sete Lagoas Fm. (fig. 2.6) towards smectite and also Fe-Mg oxide like compositions on Serra de Santa Helena and Lagoa do Jacaré fms.

In addition, the C-N-K and C-N-F ternary plots also shows that all shale samples follow the same petrographic trend (fig. 2.6) towards Al depletion and Ca, Na, K and Fe enrichments, despite anomalous Sete Lagoas Fm. K concentrations. In agreement with trace element provenance plots, ternary plots also suggest that all studied samples derive from the same common source rock, as provenance plots (fig. 2.7) shows low chemical variability between both shale and carbonate samples, pointing towards a common igneous felsic-intermediate source (figs. 2.7c,d), probably generated in neighboring contemporaneous arc systems (Paula-Santos et al., 2015).

As no provenance shift was observable among all studied samples, major element variability is probably related to different source rock interaction with the weathering regime (Nesbitt and Young, 1982). According to Kronberg et al. (1996) higher CIA values and chemical compositions towards the illite apex (e.g Carrancas Fm.), reflects a tropical weathering regime, and Lower CIA values in association with alkali and metal rich clays (e.g Serra de Santa Helena and Lagoa do Jacaré Fm.) are indicative of drier and/or colder weathering regimes. Even though these chemical differences suggest a weather shift, the low variance on CIA signal (only 68-78), coupled with weak relationship between, CIA and $\delta^{13}C$ (inverse relationships- see figure 2.5b) and CIA and

TOC (R^2=0.1), testify that climate was unlikely to be the main source of paleoenvironmental changes that took place in the Bambuí basin. Most likely, major element variability reflects only a minor paleoclimatic transition from a typical tropical regime on Carrancas and Sete Lagoas Fm. sediments to a slightly drier yet warm weather condition on Serra de Santa Helena and Lagoa do Jacaré Fm. sediments. This is in concordance with strongly negative $\delta^{18}O$ and strongly positive $\delta^{13}C$ signal from Serra de Santa Helena and Lagoa do Jacaré Fm (This work, fig. 2.5b - Paula-Santos et al., 2017) which indicates high evaporation rates and warm seawater temperature (Santos et al., 2000; Paula Santos et al., 2017). The anomalous K enrichment on Sete Lagoas Fm. sediments might be a direct result of enhanced tropical weathering (Roser and Korsch, 1988) triggered by deglaciation melt waters, though this interpretation can be easily ruled out by common shale diagenetic K enrichment (Fedo et al., 1995).

Independently from major element variability, provenance plots (fig. 2.7) show that trace elements (e.g. Ti, Th and Zr) related to the detrital (clastic) fraction are close to PAAS concentrations in all sections with almost constant values (fig. 2.5). To access the extent of detrital input on carbonates, concentrations of immobile trace elements such as Th, Zr, and Sc are good indicators, as these elements are concentrated on aluminosilicates from the detrital fraction of terrigenous input (Tribovillard, 2006; Schroder and Grotzinger, 2007). On carbonatic rocks, Frimmel (2009) used Zr vs $\sum \mathrm{REE} + \mathrm{Y}$ covariation and Zr total concentrations to track detrital contaminations, which can also be revealed by flattened, shale like REEPN patterns in association with low Y/Ho ratios close to crustal values (ca. 26-27).

A strong detrital component is identified in all studied sections. A general cross plot between Zr vs $\sum \mathrm{REE} + \mathrm{Y}$ yields a strong correlation (r^2=0.71, n=18) on carbonate samples, where deviations are related to detrital free pure carbonates from Ilcom section. $\sum \mathrm{REE} + \mathrm{Y}$ contents from impure carbonates are enriched and present high values ranging from 35 to 87 ppm (mean= 52 ppm), indicating a constant detrital contamination across the profile. This constant contamination is also verified by nearly constant Ti/Al (fig. 2.7b) ratios on both carbonate and shales coupled with covariant Ti/Al-Zr (Ti/Al-Zr R2=0.71). A general flatten pattern from REEPN plots (Fig.2.9b) of impure carbonates is also related to detrital contamination. Y/Ho ratios of carbonates are very low (carbonate mean= 29.6), which can also be associated with detrital contamination on carbonate samples.

To access direct seawater chemistry avoiding detrital contamination, only Y/Ho ratios from pure (Zr < 4 ppm) carbonates can be used. Samples IL-0 and IL-1 from Ilcom section show Zr concentrations below 4 ppm, and presents low Y/Ho ratios of 38 and 37, indicating a strong detrital

(crust derived) component on Bambuí seawater signature, following recent observations from Kuchenbecker et al. (2016), Paula Santos et al. (2018) and Caxito et al. (2018) which attributed the crustal signature of lower Bambuí seawater to a post-glacial enhanced detrital influx coupled to riverine water mixing. However, the persistence of detrital contamination on upper levels such as in the Jaíba section from Lagoa do Jacaré Formation cannot be accounted to post glaciogenic effects, suggesting that the studied sections were located close to crustal source areas and the overall Bambuí seawater chemistry was influenced by detrital influx from continental areas. On the other hand, recent evidences from Paula Santos et al. (2018) suggests that Lagoa do Jacaré Fm. carbonates record typical seawater REE patterns with higher Y/Ho ratios (up to 51) on cutoff samples bearing Sc < 0.2 µg/g. However, the presence of these detrital free carbonates is conditioned to sections located away from the mobile belts. Importantly, this sections also bears carbonates contaminated with detrital fractions, which suggests that this normal marine condition was only momentarily reached on isolated areas away from the main sediment source areas, indicating that detrital input contamination strongly influenced the chemical evolution of the Lagoa do Jacaré Fm. sediments.

Enriched via detrital input, bionutrient elements such as Ba are generally accumulated during organic matter sink and to some extent, enrichments of this element can be used to trace paleoproductivity (Babu et al., 2002, Tribovillard et al., 2006, Ma et al., 2017). To access Ba enrichment over the detrital fraction, crossplots against detrital elements Zr, Th and Sc were plotted (not shown). Moderate to weak correlations on both shale (Zr R^2 =0.84, Sc R^2=0.44, Th R^2=0.43) and carbonate samples (Zr R^2=0.55, Sc R^2=0.72, Th R^2=0.52) and strongly enriched Ba/Th ratios are coupled with enriched TOC concentrations, especially on Sete Lagoas Fm. samples (Holcim shales and both carbonate + shale from Ilcom section) (fig. 2.5) and can be a indicative of enhanced organic carbon sink and high bioproductivity on Carrancas (Ba/Th SEF=3.7) and Sete Lagoas formations (Ba/Th SEF=3.2; CEF= 19.2). Moreover, as suggested by Babu et al. (2002) and Algeo et al. (2011), using (Ba X Al) and (Ba X Zr) PAAS ratios as a detrital background average for both Shale and cabonate samples, our data confirms that Ba concentration on Carrancas and Sete Lagoas formations are strongly enriched relatively to background values, while Serra de Santa Helena and Lagoa do Jacaré formations presents depleted Ba concentrations (fig.2.8d).The $\delta^{13}C$ signal from lower Sete Lagoas Fm. carbonates (This work, fig. 2.5b and Caxito et al., 2018) do not correspond to this increased bioproductivity, as all carbonate samples yield isotopically depleted $\delta^{13}C$ values between -3 and 0‰. Nevertheless, this negative lower Sete Lagoas Fm. $\delta^{13}C$ values are firmly interpreted as the result of ^{13}C-depleted organic carbon transport by deglaciation melt waters from continental areas by several authors (Santos, 2000, Vieira et al., 2007, Caxito et al., 2012, 2018,

Paula-Santos et al, 2017), reaffirming the intrinsic relationship between post-glaciogenic melt water run-off, detrital input of bionutrient elements and high bioproductivity rates on Sete lagoas Fm. sediments.

This relationship is not verified in Serra de Santa Helena and Lagoa do Jacaré Fm. samples. Contrary to Sete Lagoas Fm. samples, Serra de Santa Helena and Lagoa do Jacaré Fm. show strongly positive $\delta^{13}C$ (between 9-15‰) (this work, fig. 2.5b - Reis, 2013; Paula Santos et al., 2017) and low TOC (Shales mean= 0.4%; Carbonates mean=0.15%) and Ba (mean SEF< 1) (fig. 2.5). This anomalously high $\delta^{13}C$ (> 10‰) values are commonly interpreted as due to a high bioproductivity episode (Reis, 2013), which would induce an anomalous fraction of buried organic carbon ($f$org) of 65.3% as calculated by Paula-Santos et al. (2017). This anomalous high $\delta^{13}C$ values however cannot be achieved with only organic matter burial. Following observations from Birgel et al. (2015) on modern lagoonal stromatolites bearing high $\delta^{13}C$ (up to 16‰), Paula-Santos et al. (2017) suggests that anomalously high $\delta^{13}C$ values on Lagoa do Jacaré Fm. carbonates can be a result of other processes such as the degradation of the organic matter by Archea activity through methanogenesis in anoxic environments with sulfate limiting conditions, coupled with the effects of ^{13}C fractionation in a stratified and stagnant watermass. As corroborated by discordant bioproductivity proxies (low TOC and Ba), it is likely that the anomalously high $\delta^{13}C$ values obtained in Lagoa do Jacaré and Sete lagoas Fm. (Santos et al., 2000, Reis, 2013, Paula-Santos et al., 2017) were achieved due to intrabasinal environmental influence (e.g watermass anoxia and restriction) rather than actual high bioproductivity.

In resume, the Bambuí Basin register a strong detrital influx which is observed in all studied sections, which can be correlated to an increased bio-nutrient input to the Bambuí basin seawater which lead to an increased bioproductivity on Sete Lagoas Fm. sediments. Conversely, this strong detrital input is not followed by bionutrient accumulation and high bioproductivity on upper stratigraphic units such as the Serra de Santa Helena and Lagoa do Jacaré fms. Our data also shows that the chemical composition of the detrital input was only weakly controlled by source-related or climatic factors, indicating that Bambuí basin sediment geochemistry was strongly controlled by internal watermass processes under the regional influence of concomitant tectonic evolution of neighboring orogenic systems.

2.5.2. Redox conditions

Black shale REE contents are generally believed to record the REE distribution from sediment source areas, as those lithotypes tend to present flattened shale-like REEPN patterns

coupled with Low Y/Ho ratios and no LREE depletions over HREE, which are strong indicatives of a detrital, non-fractionated REE source (Taylor and McLennan, 1985; Guo et al., 2007). Nevertheless, anomalous seawater-like REEPN patterns on shales are reported from the Yangtze Platform (Lehman et al.,2007; Pi et al., 2011; Li et al., 2015; Guo et al., 2016). Pi et al. (2011) show that organic matter from black shales tends to be enriched on REE, and also preserves the REE signature of seawater through authigenic enrichment. This suggests that some of the REE patterns of black shales may be originated by authigenic (nondetrital) processes, registering the seawater REE distribution to a small extent (Li et al., 2015).

Likewise, the REE pattern of Carrancas Fm. Shales should be a resultant of mixing between terrigenous and authigenic sources, and the observed REE distribution should at minor extents represent the seawater REE chemistry.

Following this observations, negative Ce anomalies (Ce/Ce* down to 0.66) are widespread on Carrancas Fm. section, which is also marked by strongly covariant enrichments of redox sensitive trace element (covariant High U/Th, V/Th and Mo/Th; figs. 2.5 and 2.8c). Sample MH1-005(A) yield a FeHr/FeT of 0.46 and FePy/FeHr of 0.002 (fig. 2.5). This apparent contradiction between redox proxies, where Ce anomalies indicate oxidizing conditions, TE enrichments and iron speciation data suggest anoxic and ferruginous conditions, is in fact a very common feature of Neoproterozoic marine basins such as in the Guizhou (Guo et al., 2007 and Goldberg et al., 2007) and Hunan provinces (Guo et al., 2016) of South China, the Otavi Group of Namibia (Rodler et al., 2016) and the Sierra Bayas Group of Argentina (Bagnoud-Velásquez et al., 2013). In those basins, these features are interpreted as a result of deposition under a layered ocean, with an oxygenated surface layer that oxides organic matter and produces the negative Ce anomalies, and a bottom anoxic/ferruginous layer where this Ce depleted organic matter accumulates and produce authigenic enrichments of redox sensitive trace elements. Following these interpretations, coupled negative Ce anomalies and enriched trace element patterns suggest that the Carrancas Fm. was deposited under a layered (stratified) seawater column. Despite the presence of bottom water anoxic/ferruginous conditions Mo concentrations are enriched relatively to PAAS values on Carrancas Fm. shales. As Mo deposition in anoxic environments is favored by the presence of $H_2S(aq)$, enrichments of these elements occur in euxinic conditions on modern seawater. This evidence suggests that Mo concentration on Carrancas Fm. was sufficiently high to allow Mo enrichment on H_2S limiting conditions, indicating that the RSE reservoir was voluminous, as observed on enriched V and U concentrations of Carrancas Fm. shales.

Contrary to the Carrancas Formation, the Sete Lagoas Formation presents a more complex redox evolution. Ce anomalies vary from slightly negative values on Ilcom section, to slightly positive values (~1.1) on Holcim section samples, and stabilizes around slightly negative (~0.9) values on Holcim section carbonates. Trace element enrichments are higher on Ilcom section and shale samples from Holcim section, presenting good covariation between U, V and Mo contents (figs. 2.5 and 2.8c), although these correlations decrease on Holcim section carbonates. Iron speciation data yield FeHr/FeT of 0.14 and FePy/FeHr of 0.3 on Sample FN-5 from Ilcom section and FeHr/FeT of 0.38 and FePy/FeHr of 0.58 on sample CX31-192 (fig. 2.5). This suggests that lower Sete Lagoas Formation seawater experienced bottom water oxygenation as indicated by Ilcom section REE and iron speciation data. This environment evolves to a typical stratified seawater featuring an oxic top layer (negative Ce anomalies - fig. 2.5) and anoxic ferruginous to euxinic bottom layer, where abundant organic matter burial and RSE enrichment took place as evidenced by Holcim section sample iron speciation, TOC and RSE data (fig. 2.5).

The Serra de Santa Helena and Lagoa do Jacaré fms., on the other hand, present positive Ce anomalies (~1.13) and lack strong U, V and Mo covariations presenting negative to muted RSE enrichment, though some covariant Ni-Cu and Mo are observed on shales (fig. 2.5). Iron speciation on sample MH2-004 from Serra de Santa Helena Fm. yield FeHr/FeT of 0.37 and FePy/FeHr of 0.03 and sample Mj002-fn02 from Lagoa do Jacaré Fm yields FeHr/FeT of 0.57 and FePy/FeHr of 0.15. Unlike Carrancas and Sete Lagoas formations, middle Bambuí stratigraphic units lack strong evidence of RSE enrichment and organic matter burial (e.g low TOC values - fig. 2.5), though REE and iron speciation data suggest sediment deposition under dysoxic, probably anoxic/ferruginous conditions (fig. 2.5). As verified on Carrancas Fm. shales, discrepancies between RSE enrichments and redox conditions are observed on Lagoa do Jacaré Fm. negative and muted U and especially V enrichments that are inconsistent with anoxic and ferruginous water conditions (Miller et al., 2017), indicating that RSE availability on Lagoa do Jacaré Fm. seawater was probably low.

2.5.3. Bambuí basin paleoenvironmental evolution

According to the geochemical groups described on REE distribution, we divide the evolution of Bambuí basin seawater based on REE and TE distributions as follows:

Carrancas Formation (Section 1)

Samples from the Carrancas Formation show a very uniform and distinct geochemical pattern. Differently from other stratigraphic units of Bambuí group, the Carrancas Fm. presents REEPN patterns of typical Neoproterozoic open marine seawater (fig. 2.9a) including Higher Y/Ho

ratios, MREE and HREE enrichment over LRRE, and negative Ce anomalies coupled with redox sensitive trace element enrichments which seems to be indicative of a stratified watermass.

Whereas it is impossible to know the exact seawater chemistry on which sediments from Carrancas were deposited (See section 2.5.2), we can access seawater chemical structure by analyzing RSE enrichments and iron speciation data which are reliable proxies. These proxies show that Carrancas seawater presents a typical stratified structure featuring an oxygenated top layer and a bottom anoxic/ferruginous layer, like most of Neoproterozoic open marine systems, which inarguably shows that despite uncommon seawater-like REE and a strong detrital contamination, Carrancas Fm. shales were deposited in a stable marine system. In fact, on U-Mo EF plots from Algeo & Tribovillard (2009) and on Cd/Mo-Co/Mn plots from Sweere et al. (2016) (fig. 2.10) the plotting of the samples suggest that Carrancas Fm. was probably deposited in an open marine setting (See fig. 2.10 caption for further explanations). These observations are also concordant with recent observations from Uhlein et al. (2016), which suggest that the Carrancas Fm. composes a pre-Marinoan glaciogenic rift-related intracratonic connected marine system that preceded the Bambuí Group deposition.

Despite the inarguably strong evidences on the presence of a typical Neoproterozoic seawater stratification on Carrancas Fm. shales deposition, Mo enrichments observed in this section remains an intriguing question. As Mo authigenic enrichments on sediments are induced by the presence of $H_2S(aq)$, this Mo enrichments must be the result of TE enrichment during small euxinic episodes on which sufficient $H_2S(aq)$ was available to promote Mo complexation and uptake on sediments. In fact, dominant bottom water ferruginous conditions alternated with small episodes of euxinia are in fact very characteristic of Neoproterozoic basins (Canfield et al., 2007; Johnston et al., 2010). Whereas the origin of redox conditions in the Carrancas Fm. are difficult to interpret, the anomalous RSE enrichments on Carrancas Fm. shales indicate that RSE was readily available on pre-Marinoan Carrancas Fm. seawater. Nevertheless, it is very difficult to access if this high RSE availability was induced by atmospheric oxygenation (e.g Doushantuo Fm., Sahoo et al., 2012), or if its contents just reflect the detrital background of the basin (e.g Mackenzie Mountains Supergroup, Miller et al., 2017) without further study of other proxies.

Bambuí Group - Ilcom, Holcim, Papagaios and Jaiba sections (2-5) (Figure 2.11)

The paleoenvironmental evolution of the Bambuí basin is summarized on figure 2.11. Contrary to Carrancas Fm., samples from both Ilcom and Holcim sections are chemically heterogeneous. Both impure (Zr > 4ppm) carbonatic rocks and shales are characterized by High $\sum \mathrm{REE} + \mathrm{Y}$ contents, flattened $\mathrm{REE_{PN}}$ patterns coupled with lower Y/Ho ratios, and high detrital TE

concentrations, which suggests a strong detrital component on seawater (figs. 2.5 and 2.9). Pure carbonate samples (IL-0, IL-1), prone to register direct seawater chemistry, present an uncommon REEPN pattern with strong HREE depletion over MREE enrichment with higher, but still crustal-like Y/Ho (38.2 and 37.2) values. Ce anomalies are oscillating over Ilcom section and on lower Holcim, being constant at upper Holcim carbonates. Redox sensitive TE, especially U, V and Mo are markedly enriched at Ilcom section and on lower Holcim shales, and depleted at upper Holcim carbonates (fig. 2.5).

These features suggest that Sete Lagoas Fm. deposition was marked by a very unstable initial phase with oscillating oxygenation pulses suggested by iron speciation data, pointing towards oxygenated bottom waters on Ilcom shale samples. This oscillating stage on the lower Sete Lagoas Fm. is also accompanied by strong negative $\delta^{13}C$ anomalies which are related to a post glacial ice water influx (fig. 2.5b- Vieira et al., 2007; Caxito et al., 2012; Kuchenbecker et al., 2016). In this post glacial scenario, it is likely that ice water discharge from the continent would cause drastic changes on marine seawater affecting the carbon cycle by negative $\delta^{13}C$ carbon input, organic bioproductivity by micro-nutrient input influx and oxi-redox conditions by an initial seawater oxygenation (fig. 2.11- Hoffman and Schrag, 2002; Frei et al., 2011).

REE, TE and TOC enrichments patterns shows that lower Bambuí samples were indeed strongly affected by ice meltwater influx, registering oscillating $\delta^{13}C$ values, increased bioproductivity (high Ba/Th; high TOC), oscillant oxi-redox conditions (oscillating Ce anomalies coupled with TE enrichments and FeHr/FeT < 0.22 fig. 2.5), and strong continental detrital influence (crustal REE and Y/Ho signatures (figs. 2.5 and 2.9). This marine oxygenation and enhanced bioproductivity following deglaciation is commonly associated with the rising of atmospheric oxygen levels and the proliferation of Ediacaran fauna (Hofmann and Schrag, 2002; Och and Shields-Zhou, 2012) on Neoproterozoic basins. In agreement with our data, based on $\delta^{53}Cr$ data, Caxito et al. (2018) suggest that protracted seawater oxygenation was reached on lower Sete Lagoas Fm., locally representing a global oxygenation phenomenon registered in several contemporaneous post-Marinoan deposits (Caxito et al., 2018 and references therein). This protracted oxygenation may also have led to complex life diversification in the Late Ediacaran, as represented by Cloudina sp. remnants found in the middle portion of Sete Lagoas Fm. (Warren et al., 2014). This timespan is also marked by the increase of RSE availability on marine seawater, as registered by peak anomalous RSE enrichments observed in diverse basins (Och and Shields-Zhou, 2012 and references therein), which are interpreted as an effect of enhanced oxidative continental weathering and protracted RSE input on marine basins (Sahoo et al., 2012). High RSE enrichments observed in Sete Lagoas Fm. samples may be associate with this increase on atmospheric oxygen

levels, although care is needed as this high yet not huge enrichments can represent only local TE background values masked by authigenic enrichment induced by anoxic seawater conditions (Miller et al., 2017). As RSE elements are also enriched on the Carrancas Fm. shales, which are believed to be deposited before the Marinoan Glaciation in the São Francisco basin (Uhlein et al., 2016), it is almost impossible to access whether these enrichments represent the effects of enhanced oxidative weathering or just the local TE background. Most likely, oxygenation pulses only enhanced an already high RSE local reservoir.

After this unstable initial phase following post-glaciogenic effects, high bioproductivity on surface waters leads to enhanced organic matter burial sink (Hofmann and Schrag, 2002). The accumulation of organic matter on bottom waters, in turn, promote anoxia by consuming the available oxygen in the OM degradation process (Johnston et al., 2010; Ma et al., 2017), leading back to a stratified Neoproterozoic seawater (fig. 2.11). Our iron speciation data from the Holcim section yield anoxic conditions with high FePy/FeHr = 0.6, suggesting high pyrite burial rates and indicating possible euxinic excursions. As verified on Carrancas Fm. shales, Mo enrichments on Sete Lagoas Fm. shales also indicates short euxinic excursions on bottom water. This environmental cycle following deglaciation is also marked by seawater chemical stabilization, including an increase on $\delta^{13}C$ values (from -3‰ to 0‰ - fig. 2.5b), surface water oxygenation presenting stable Ce/Ce* values which indicate no anomaly (around 0.9) and diminished bioproductivity (Caxito et al., 2018). REE patterns also tend to lost crustal influence and evolve back to typical marine signatures (Frimmel, 2009; Rodler et al., 2016). This recovery also involves large scale marine transgression, which evolves from restricted and shallow deposits immediately after deglaciation to modern like open marine settings (Vieira et al., 2007, Paula-Santos et al., 2017). This cycle is registered on U-Mo EF plots from Algeo & Tribovillard (2009) and on Cd/Mo-Co/Mn plots from Sweere et al. (2016), where Ilcom samples plots indicates deposition in a more restricted setting, evolving to more open and less restricted marine settings on Holcim section samples plots (fig. 2.10). This observation is in strong agreement with recent data from Caxito et al. (2018) and Paula-Santos et al. (2017, 2018), which suggest that the Sete Lagoas Fm. depositional environment evolves from a restricted unstable post glaciogenic basin towards an open and stable marine system where sufficient coastal surface, watermass circulation and oxygenation was reached to allow Cloudina sp. irradiation (fig. 2.11- Warren et al., 2014). Independently from its paleoenvironmental evolution, REE pattern from Holcim section samples are still highly influenced by continental detrital input (flat REEPN, high $\sum REE + Y$ contents and low Y/Ho - fig. 2.9) showing that continental detrital influx was still affecting sediment geochemistry long after the post glaciogenic stage (Kuchenbecker et al., 2016; Paula-Santos et al., 2017; Caxito et al., 2018). This suggests that

the evolution of Bambuí seawater was tied to crustal influence due to its localization inside a cratonic area surrounded by Neoproterozoic belts (figs. 2.1 and 2.11) independently from post-glaciogenic melt water influx.

As such, crustal-like REE signatures are also present on Serra de Santa Helena and Lagoa do Jacaré formations samples. Unlike other contemporaneous Neoproterozoic marine basins such as Sierra Bayas Group (Bagnoud-Velásquez et al., 2013); Corumbá Group (Spangeberg et al., 2014) and Otavi Group (Frimmel, 2009 and Rodler et al., 2016), upper stratigraphic units from the Bambuí basin lacks distinctive seawater REE signatures (fig. 2.9) which are indeed marked by strong crustal detrital influence (this work and Kuchenbecker et al., 2016 - See section 5.1). Despite a similar crustal-like REE pattern, major environmental differences are observed on upper Bambuí samples (Serra de Santa Helena and Lagoa do Jacaré Fm.). Firstly, the layered seawater structure of middle Sete Lagoas Fm. gives place to anoxic ferruginous (FeHr/FeT of 0.57 and FePy/FeHr of 0.15) watermass that yield strongly positive Ce (up to Ce/Ce* = 1.3) anomalies even on shallow carbonate samples (this work, Paula Santos et al., 2018), indicating possible shallow water anoxia. Despite strongly anoxic conditions, RSE presents muted or even negative enrichment factors. Beyond Mo, which depends on euxinic conditions, and U which is enriched via organic matter complexation (see section 1.2.2), no authigenic related factor explains muted V enrichments, as enrichments of this element were abundant on stratigraphic lower units, and crustal detrital input remained constant as indicated by detrital proxies (see section 2.5.1- figs. 2.5 and 2.7). A possible decrease on continental oxidative weathering by diminished oxygen release might be associated with decreased RSE influx to seawater, though detrital input is observably constant, and the protracted oxidative weathering model is not evident in any of these samples, thus ruling out this interpretation.

Importantly, this decrease in the RSE reservoir is accompanied by lower TOC and bionutrient TE enrichments, suggesting that Upper Bambuí stratigraphic units were also marked by low productivity. This low bioproductivity is explained by the restriction model proposed by Paula Santos et al. (2017). In this scenario, stagnant watermass would favor ^{13}C fractionation (Santos et al., 2000), which is also favored by the result of other processes such as the degradation of the organic matter by archea activity through methanogenesis in anoxic environments with sulfate limiting conditions proposed by Paula Santos et al. (2017) following the observations on recent coastal lagoonal stromalites taken by Birgel et al. (2015). In this model, the lack of connection with open marine seawater strongly decreases the sulfate supply to the restricted watermass, promoting one of the necessary biochemical conditions to promote anomalously high ^{13}C fractionation patterns (fig. 2.5b) observed on Lagoa do Jacaré Fm. carbonates. Low sulfate supply in the other hand,

would inhibit bacterial sulfur reduction, favoring widespread ferruginous conditions (Johnston et al., 2010). This processes is affirmed by iron speciation and high (above 0.8) FeT/Al ratios registered on Lagoa do Jacaré Fm shales, indicating widespread anoxic and ferruginous watermass conditions, which were also favored by protracted continental detrital input of terrigenous material elevating Fe concentrations on seawater. In concordance with recent data, the presence of ferruginous conditions in Lagoa do Jacaré Fm. was already suggested by Uhlein et al. (2017). Lastly, U-Mo EF plots from Algeo & Tribovillard (2009) and on Cd/Mo-Co/Mn plots from Sweere et al. (2016) (fig. 2.10), also indicates that both Serra de Santa Helena and Lagoa do Jacaré Fm. shales were likely deposited in a restricted and stagnant watermass setting (See fig. 2.10 captions for further explanations). The restriction model also explains the lack of RSE enrichments, which can be related to a low watermass TE re-supply rates, as this disconnected watermass would not homogenize its TE inventory with an open marine source, explaining the low abundances of RSE, bionuntrient TE and most importantly dissolved oxygen (as suggested by surface waters anoxia - fig. 2.5), which ultimately lead to a diminished bioproductivity and low biological diversification, as verified by the lack of an evolved eukaryotic fauna in upper Bambuí stratigraphic units.

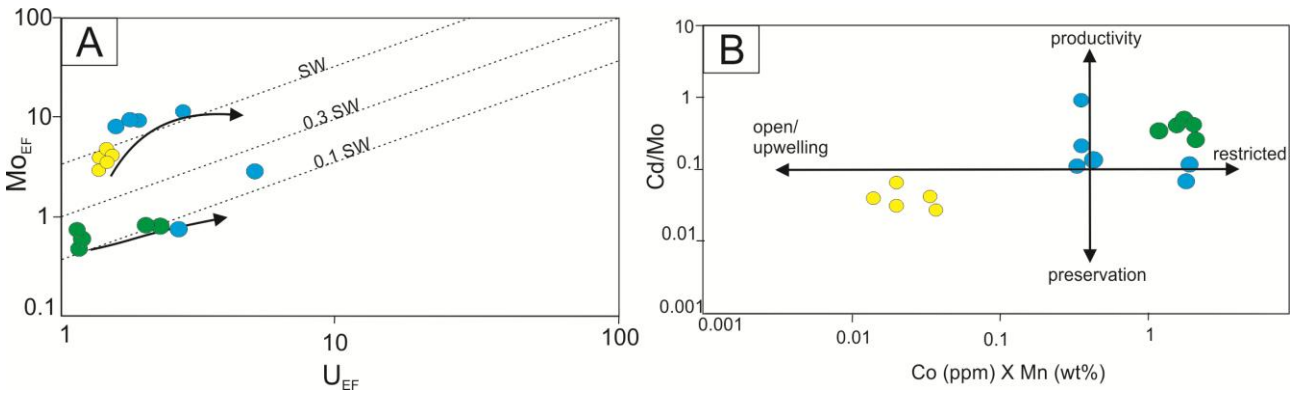

Fig 2.10 A) Mo-U covariation plot from Algeo and Tribovillard (2009). Carrancas Fm. plots featuring higher MoEF and Low UEF represent a typical marine evolution of a weakly restricted basin. While samples from Ilcom section falls on the suboxic evolution (low Mo and high U EF), Holcim section samples suggest an watermass evolution from weakly restricted towards watermass restriction. At last, Lagoa do Jacaré Fm.presents Low Mo and U EF which are caused by watermass strong restriction (See text for details) B) Cd/Mo x Co/Mn covariation plots from Sweere et al. (2016).

2.5.4. Paleoenvironmental implications for Neoproterozoic intracontinental basins

Like most Neoproterozoic basins, the Bambuí basin sediment geochemistry registers a typical stratified watermass setting featuring an oxygenated superficial layer and a predominant anoxic/ferruginous bottom layer which episodically turned to euxinic conditions and some episodic deep water oxygenation following deglaciation. Despite its similar redox structure, the Bambuí

basin features intriguing RSE data, which seems disconnected from the redox structure of the seawater. In fact, the Bambuí basin RSE reservoir seems to be influenced by local background values, with minor contributions of episodic enhanced oxidative weathering. Following Kunzmann et al. (2015) and Miller et al. (2017), our data suggests that RSE enrichments are strongly controlled by local background values, indicating that RSE data can't be evaluated without other proxies such as iron speciation, $\delta^{53}Cr$ or $\delta^{34}S$ when analyzing great oxygenation events (Fike et al., 2006; Frei et al., 2011; Caxito et al., 2018). Nevertheless, recent contributions suggest that the Bambuí basin (specifically the lower-middle Sete Lagoas Fm.) records a protracted oxygenation event following deglaciation (this work and Caxito et al., 2018).

Due to its intracratonic nature (figs. 2.1 and 2.11), the Bambuí basin presents several interesting singularities that are directly related to Neoproterozoic paleoenvironmental evolution. Firstly, all analyzed samples are marked by a high continental detrital input signal independently from oxidative continental weathering and deglaciation melt water runoff. Whereas it is not possible to observe other environmental changes rather than the increase of bionutrient TE input, Mackey et al. (2017) show that mud deposition reduces stromatolite complexity, suggesting that detrital input may interfere on live organism evolution. Even though this possibility can't be evaluated in our samples, the low biological variability and high continental detrital input verified in our study rise interesting future possibilities for the study of intracratonic marine systems. Apart from Carrancas and Sete Lagoas Fm. which seems to be connected to some extent to external open marine watermasses (fig. 2.11- Warren et al., 2014; Paula Santos et al., 2015, 2017, 2018), both Serra de Santa Helena and Lagoa do Jacaré Fm. present an isolated evolution, within a restricted watermass. This isolated evolution influenced all geochemical proxies, including discordant $^{87}Sr/^{86}Sr$ and $\delta^{13}C$ signatures (Caxito et al., 2012; Paula-Santos et al., 2015, 2017) and also Low TOC and RSE values. The lack of connection with open marine seawater primarily decrease sulfate re-supply, favoring widespread ferruginous conditions even at surface waters. The lack of re-supply also affects bionuntrient and RSE input, which may reduce bioproductivity, affecting the biologic cycle. Most importantly, our data suggest that the lack of re-supply also affected the dissolved oxygen content of the watermass, which may have inhibited the so-called Cambrian life explosion (Maruyama and Santosh, 2008) registered worldwide, in the upper Bambuí basin.

Our data suggest that the current Neoproterozoic-Cambrian transition model featuring oceanic oxygenation and complex life explosion (Maruyama and Santosh, 2008) depends on a connected watermass where the re-supply of sulfate, trace elements and dissolved oxygen is effective in coastal areas, allowing proper bionuntrient consumption by live organisms, inducing

bioproductivity and consequent biological evolution. In this model global tectonics play a significant role, as the closure and opening of marine basins during the late stages of Rodinia breakup and Gondwana amalgamation favored the installation of large coastal platform areas, favoring the Cambrian life explosion (Braiser and Linsday 2001; Meert and Liebermann, 2008). At last, our data suggest that discrepancies in the geochemical signature of Neoproterozoic sediments may be related to local tectonic features, and care is needed when inferring global events from individual sediment geochemical records.

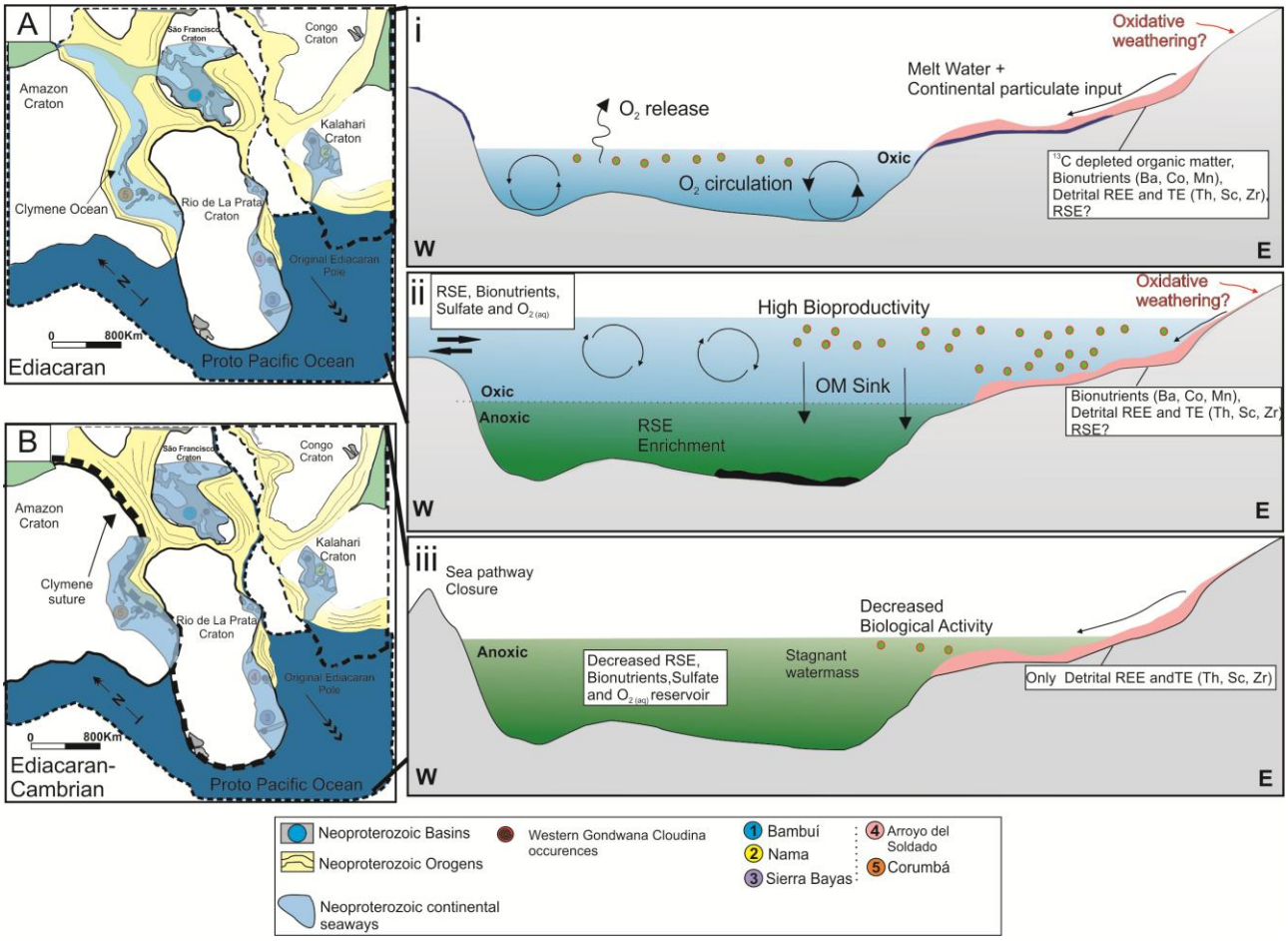

Fig 2.11. Probable paleogeographic (based on Misi et al. (2005) and Alkmim et al. (2006) and paleoenvironmental (this work) scenario of western Gondwana during the Cambrian-Ediacaran transition (i) Summarizes the environmental features of lower Sete Lagoas Fm. (Ilcom section). (ii) Summarizes the environmental features of middle Sete Lagoas Fm. (Holcim section) (ii) Represents the environmental scenario from upper Bambuí basin stratigraphies (Serra de Santa Helena and Lagoa do Jacaré Fm.). A) Following Neoproterozoic glaciations (i- Lower Sete Lagoas Fm.), western Gondwana basins were liked connected by continental seaways (Tohver et al., 2010, 2012; Warren et al., 2014; Paula-Santos et al., 2017), which were related to appearance of *cloudina sp.* and typical open marine environments that can be observed on middle Sete Lagoas Fm. (ii). B) During the Ediacaran-Cambrian transition, these seaways were disconnected by tectonic activity, isolating the São Francisco Basin, which evolved in a restricted environmental scenario as suggested by Lagoa do Jacaré Fm. data (iii).

2.6) Conclusions

In summary, the data presented in this contribution shows that:

1) A strong detrital contamination is observed in almost all studied sections. This enhanced detrital influx could lead to an increased bioproductivity on both Carrancas Fm. and lower Bambuí group stratigraphic units, though no other environmental effects were verified. Provenance data show that despite strong continental detrital input rates from surrounding orogens, all studied sediments probably share a common source rock, and small changes on the weathering regime are not likely to have influenced RSE and TE geochemistry.

2) Iron speciation data, Ce anomalies and RSE enrichments show that the Carrancas Fm. was deposited in typical open marine stratified setting, while the lower Bambuí (Sete Lagoas Fm.) experienced a very unstable initial stage marked by protracted oceanic and possibly atmospheric oxygenation, followed by a stable open marine-like stage featuring high bioproductivity on shallow waters and euxinic incursions on predominant anoxic/ferruginous bottom waters. On the other hand, the upper Bambuí stratigraphic units (Serra de Santa Helena and Lagoa do Jacaré fms.) register marine evolution in a restricted scenario, where anoxic ferruginous conditions probably reached surficial waters. The RSE reservoir of the Bambuí basin was primarily controlled by already high background values and local environmental factors (e.g watermass restriction), and despite evidences of protracted oceanic and possibly atmospheric oxygenation, no signal of enhanced continental oxidative weathering and consequent RSE marine influx were registered.

3) Major environmental and biological changes are registered on the upper Bambuí stratigraphic units. The lack of oceanic connection prevent the re-supply of marine sulfate, RSE, bionutrients such as Ba and ultimately of dissolved oxygen. This inefficient and poorly supplied marine system decreased biological activity and probably damaged biological evolution, preventing the rise of a typical Cambrian ecosystem.

4) Our data suggest that oceanic connectivity and proper re-supply of inorganic marine input were fundamental keystones in the development of complex life formation in the Ediacaran-Cambrian transition. Furthermore, local tectonics played an important role on this transition by creating large coastal and platformal areas supplied by open marine sources, as opposed to small and disconnected intracratonic marine systems which would inhibit biological diversification. This suggests that the geochemical and biological evolution of Neoproterozoic basins are firmly related to local tectonic context, and care is needed when inferring global environmental events from only local data.

REFERENCES

Algeo, T. J., 2004. Can marine anoxic events draw down the trace element inventory of seawater?. Geology, 32(12), 1057-1060.

Algeo, T. J., & Maynard, J. B., 2004. Trace-element behavior and redox facies in core shales of Upper Pennsylvanian Kansas-type cyclothems. Chemical geology, 206(3), 289-318.

Algeo, T. J., & Tribovillard, N., 2009. Environmental analysis of paleoceanographic systems based on molybdenum–uranium covariation. Chemical Geology, 268(3-4), 211-225.

Algeo, T. J., Kuwahara, K., Sano, H., Bates, S., Lyons, T., Elswick, E., Maynard, J. B., 2011. Spatial variation in sediment fluxes, redox conditions, and productivity in the Permian–Triassic Panthalassic Ocean. Palaeogeography, Palaeoclimatology, Palaeoecology, 308(1-2), 65-83.

Almeida, F.F.M., 1977. O Cráton do São Francisco. Revista Brasileira de Geociências 7, 349–364.

Alvarenga, C.J.S., Della Giustina, M.E.S., Silva, M.G.C., Santos, R.V., Gioia, S.M.C., Guimarães, E.M., Dardenne, M.A., Sial, A.N., Ferreira, V.P., 2007. Variac¸ ões dos isótopos de C e Sr em carbonatos pré e pós-glaciac¸ ão Jequitaí (Esturtiano) na região de Bezerra-Formosa, Goiás. Revista Brasileira de Geociências 37, 147–155.

Alvarenga, C.J.S., Santos, R.V., Vieira, L.C., Lima, B.A.F., Mancini, L.H., 2014. Meso-Neoproterozoic isotope stratigraphy on carbonates platforms in the Brasília Belt of Brazil. Precambrian Res. 251, 164-180.

Alkmim, F.F., Martins-Neto, M.A., 2001. A bacia intracratônica do São Francisco: Arcabouc¸ o Estrutural e cenários evolutivos. In: Pinto, C.P., Martins-Neto, M. (Eds.). A Bacia do São Francisco geologia e recursos naturais. SBG, Belo Horizonte, pp. 9–30.

Alkmim, F. F., & Martins-Neto, M. A., 2012. Proterozoic first-order sedimentary sequences of the São Francisco craton, eastern Brazil. Marine and Petroleum Geology, 33(1), 127-139.

Arrouy, M. J., Warren, L. V., Quaglio, F., Poiré, D. G., Simões, M. G., Rosa, M. B., & Peral, L. E. G., 2016. Ediacaran discs from South America: probable soft-bodied macrofossils unlock the paleogeography of the Clymene Ocean. Scientific Reports, 6.

Babinski, M., Van Schmus, W.R., Chemale, F., 1999. Pb–Pb dating and Pb isotope geochemistry of Neoproterozoic carbonate rocks from the São Francisco basin, Brazil: implications for the

mobility of Pb isotopes during tectonism and metamorphism. Chemical Geology 160, 175–199.

Babinski, M., Vieira, L.C., Trindade, R.I.F., 2007. Direct dating of the Sete Lagoas cap carbonate (Bambuı Group, Brazil) and implications for the Neoproterozoic glacial events. Terra Nova 19, 401–406.

Babu, C. P., Brumsack, H. J., Schnetger, B., & Böttcher, M. E., 2002. Barium as a productivity proxy in continental margin sediments: a study from the eastern Arabian Sea. Marine Geology, 184(3), 189-206.

Bagnoud-Velásquez, M., Spangenberg, J. E., Poiré, D. G., & Peral, L. G., 2013. Stable isotopes (S, C) and hydrocarbon biomarkers in Neoproterozoic sediments of the Sierras Bayas Group. Argentina: Precambrian Research, 231, 388-400.

Banner, J.L., Hanson, G., Meyers, W., 1988. Rare earth element and Nd isotopic variations in regionally extensive dolomites from the Burlington–Keokuk Forma-tion (Mississippian): implications for REE mobility during carbonate diagenesis. J.Sediment. Res.58, 415–432

Bertoni, M. E., Rooney, A. D., Selby, D., Alkmim, F. F., & Le Heron, D. P., 2014. Neoproterozoic Re–Os systematics of organic-rich rocks in the São Francisco Basin, Brazil and implications for hydrocarbon exploration. Precambrian Research, 255, 355-366.

Birgel, D., Meister, P., Lundberg, R., Horath, T. D., Bontognali, T. R. R., Bahniuk, A. M., McKenzie, J. A., 2015. Methanogenesis produces strong 13C enrichment in stromatolites of Lagoa Salgada, Brazil: a modern analogue for Palaeo-/Neoproterozoic stromatolites?. Geobiology, 13(3), 245-266.

Bolhar, R., & Van Kranendonk, M. J., 2007. A non-marine depositional setting for the northern Fortescue Group, Pilbara Craton, inferred from trace element geochemistry of stromatolitic carbonates. Precambrian Research, 155(3), 229-250.

Brasier, M. D., & Lindsay, J. F., 2001. Did supercontinental amalgamation trigger the “Cambrian Explosion”. The Ecology of the Cambrian Radiation. Columbia University Press, New York, 69-89.

Broecker, W. S., & Peng, T. H., 1982. Tracers in the Sea.

Brumsack, H. J., 2006. The trace metal content of recent organic carbon-rich sediments: implications for Cretaceous black shale formation. Palaeogeography, Palaeoclimatology, Palaeoecology, 232(2), 344-361.

Canfield, D.E., Raiswell, R., Westrich, J.T., Reaves, C.M., Berner, R.A., 1986. The use of chromium reduction in the analysis of reduced inorganic sulfur in sediments and shales. Chem. Geol. 54, 149–155.

Canfield, D.E., Poulton, S.W., Narbonne, G.M., 2007. Late-Neoproterozoic deep-ocean oxygenation and the rise of animal life. Science 315 (5808), 92–95.

Canfield, D. E., Poulton, S. W., Knoll, A. H., Narbonne, G. M., Ross, G., Goldberg, T., & Strauss, H., 2008. Ferruginous conditions dominated later Neoproterozoic deep-water chemistry. Science, 321(5891), 949-952.

Caxito, F.A., Halverson, G.P., Uhlein, A., Stevenson, R., Dias, T.G., Uhlein, G.J., 2012. Marinoan glaciation in east central Brazil. Precambrian Res. 200e203, 38e58.

Caxito, F. A., Frei, R., Uhlein, G. J., Dias, T. G., Árting, T. B., & Uhlein, A. (2018). Multiproxy geochemical and isotope stratigraphy records of a Neoproterozoic Oxygenation Event in the Ediacaran Sete Lagoas cap carbonate, Bambuí Group, Brazil. Chemical Geology, 481, 119-132.

Chaves, M.L.S., Guimarães, J.T., Andrade, K.W., 2010. Litofácies glaciomarinhas na Formac¸ ão Jequitaí: possíveis implicações na redistribuição de diamantes a oeste da Serra do Espinhaço (MG). Revista Brasileira de Geociências 40 (4), 516–526.

Chiavegatto, J.R.S; Gomes, N.S.; Dardenne, M.A.; Delgado, C.E.R. 2003. Estratigrafia do Grupo Bambuí nas regiões Norte de Minas Gerais: uma nova unidade estratigráfica e um contexto de inversão de bacia. In: 12º Simpósio de Geologia de Minas Gerais, Ouro Preto.

Collins, A.S., Pisarevsky, S.A., 2005. Amalgamating eastern Gondwana: the evolution of the Circum-Indian Orogens. Earth-Science Reviews 71 (3–4), 229–270.

Conway Morris, S., 2006. Darwin's dilemma: the realities of the Cambrian 'explosion'. Philosophical Transactions of the Royal Society B: Biological Sciences 361 (1470), 1069–1083.

Costa, M.T., Branco, J.R., 1961. Roteiro para a excursão Belo Horizonte-Brasília. 14◦ Congresso Brasileiro de Geologia. UFMG, Inst. Pesq. Radioat., Publ. 15, 25p., Belo Horizonte.

Cox, G. M., Jarrett, A., Edwards, D., Crockford, P. W., Halverson, G. P., Collins, A. S., Li, Z. X. , 2016. Basin redox and primary productivity within the Mesoproterozoic Roper Seaway. Chemical Geology, 440, 101-114.

Craig, H., 1957. Isotopic standards for carbon and oxygen and correction factors for mass-spectrometric analysis of carbon dioxide. Geochimica et cosmochimica acta, 12(1-2), 133-149.

Crockford, P. W., Hodgskiss, M. S., Uhlein, G. J., Caxito, F., Hayles, J. A., & Halverson, G. P., 2017. Linking paleocontinents through triple oxygen isotope anomalies. Geology.

Cukrov, N., Alvarenga, C.J.S., Uhlein, A., 2005. Litofácies da glaciac¸ ão neoproterozóica nas porc¸ ões sul do cráton do São Francisco: Exemplos de Jequitaí (MG) e Cristalina (GO). Revista Brasileira de Geociências 35 (1), 69–76.

D'Agrella-Filho, M.S., Babinski, M., Trindade, R.I.F., Van Schmus, W.R., Ernesto, M., 2000. Simultaneous remagnetization and U–Pb isotope resetting in Neoproterozoic carbonates of the São Francisco craton, Brazil. Precambrian Research 99, 179–196.

Dardenne, M.A., 1978. Síntese sobre a estratigrafia do Grupo Bambuí no Brasil Cen-tral. In: Congresso Brasileiro de Geologia, 30, Recife, 1978. Anais., SBG, 2, pp. 597–610.

Dardenne, M.A., 2000. The Brasília Fold Belt. In: Cordani, U.G., Milani, E.J., Thomaz, A., Filho & Campos, D.A. 2000. Tectonic evolution of South America. Rio de Janeiro, SBG, pp. 231–263

Elie, M., Nogueira, A.C.R., Nédélec, A., Trindade, R.I.F., Kenig, F., 2007. A red algal bloom in the aftermath of the Marinoan Snowball Earth. Terra Nova 19 (5), 303–308.

Erickson, B. E., & Helz, G. R., 2000. Molybdenum (VI) speciation in sulfidic waters:: stability and lability of thiomolybdates. Geochimica et Cosmochimica Acta, 64(7), 1149-1158.

Fike, D. A., Grotzinger, J. P., Pratt, L. M., & Summons, R. E., 2006. Oxidation of the Ediacaran ocean. nature, 444(7120), 744.

Fedo, C. M., Wayne Nesbitt, H., & Young, G. M., 1995. Unraveling the effects of potassium metasomatism in sedimentary rocks and paleosols, with implications for paleoweathering conditions and provenance. Geology, 23(10), 921-924.

Floyd, P.A., Leveridge, B.E., 1987. Tectonic environment of the Devonian Gramscatho Basin, South Cornwall: framework mode and geochemical evidence from turbiditic sandstones. J. Geol. Soc. Lond. 144, 53–542

Frei, R., Gaucher, C., Døssing, L.N., Sial, A.N., 2011. Chromium isotopes in carbonates – A tracer for climate change and for reconstructing the redox state of ancient seawater. Earth Planet. Sci. Lett. 312, 114–125.

Frimmel, H. E., 2009. Trace element distribution in Neoproterozoic carbonates as palaeoenvironmental indicator. Chemical Geology, 258(3), 338-353.

Frimmel, H.E., 2010. On the reliability of stable carbon isotopes for Neoproterozoic chemostratigraphic correlation. Precambr. Res. 182, 239–253.

German, C. R., & Elderfield, H., 1990. Application of the Ce anomaly as a paleoredox indicator: the ground rules. Paleoceanography, 5(5), 823-833.

Goldberg, T., Strauss, H., Guo, Q., Liu, C., 2007. Reconstructing marine redox conditions for the Early Cambrian Yangtze Platform: evidence from biogenic sulphur and organic carbon isotopes. Palaeogeography, Palaeoclimatology, Palaeoecology 254, 175–193.

Gómez-Peral, L. E., Sial, A. N., Arrouy, M. J., Richiano, S., Ferreira, V. P., Kaufman, A. J., & Poiré, D. G., 2017. Paleo-climatic and paleo-environmental evolution of the Neoproterozoic basal sedimentary cover on the Río de La Plata Craton, Argentina: Insights from the δ 13 C chemostratigraphy. Sedimentary Geology, 353, 139-157.

Guilbaud, R., Poulton, S. W., Butterfield, N. J., Zhu, M., & Shields-Zhou, G. A., 2015. A global transition to ferruginous conditions in the early Neoproterozoic oceans. Nature Geoscience, 8(6), 466.

Guo, Q., Shields, G.A., Liu, C., Strauss, H., Zhu, M., Pi, D., Goldberg, T., Yang, X., 2007. Trace element chemostratigraphy of two Ediacaran–Cambrian successions in South China: implications for organosedimentary metal enrichment and silicification in the early Cambrian. Palaeogeography Palaeoclimatology Palaeoecology 254, 194–216.

Guo, Q., Deng, Y., Hippler, D., Franz, G., & Zhang, J., 2016. REE and trace element patterns from organic-rich rocks of the Ediacaran–Cambrian transitional interval. Gondwana Research, 36, 94-106.

Halverson, G. P., Wade, B. P., Hurtgen, M. T., & Barovich, K. M., 2010. Neoproterozoic chemostratigraphy. Precambrian Research, 182(4), 337-350.

Hayashi, K., Fujisawa, H., Holland, H.D., Ohmoto, H., 1997. Geochemistry of ~1.9 Ga sedimentary rocks from northeastern Labrador, Canada. Geochim. Cosmochim. Acta 61, 4115–4137.

Hoffman, P.F., Schrag, D.P., 2002. The Snowball Earth hypothesis: testing the limits of global change. Terra Nova 14 (3), 129–155.

Huerta-Diaz, M. A., & Morse, J. W., 1990. A quantitative method for determination of trace metal concentrations in sedimentary pyrite. Marine Chemistry, 29, 119-144

Isotta, C.A.L., Rocha-Campos, A.C., Yoshida, R., 1969. Striated pavement of the Upper Precambrian glaciation in Brazil. Nature 222, 466–468.

Iyer, S. S., Babinski, M., Krouse, H. R., & Chemale Jr, F.,1995. Highly 13C-enriched carbonate and organic matter in the Neoproterozoic sediments of the Bambuí Group, Brazil. Precambrian Research, 73(1-4), 271-282.

Johnston, D. T., Poulton, S. W., Dehler, C., Porter, S., Husson, J., Canfield, D. E., & Knoll, A. H., 2010. An emerging picture of Neoproterozoic ocean chemistry: Insights from the Chuar Group, Grand Canyon, USA. Earth and Planetary Science Letters, 290(1-2), 64-73.

Karfunkel, J., Hoppe, A., Noce, C.M., 2002. Serra da Água Fria e vizinhancas, MG: vestí-gios de glaciac¸ ão neoproterozóica. In: Schobbenhaus, C., Campos, D.A., Queiroz, E.T., Winge, M., Berbert-Born, M. (Eds.), Sítios Geológicos e Paleontológicos do Brasil, 1. DNPM, Brasília, Brazil, pp. 165–173.

Kirschvink, J.L., et al., 2000. Paleoproterozoic Snowball Earth: extreme climatic and geochemical global change and its biological consequences. Proceedings of the National Academy of Sciences of the United States of America 97 (4), 1400–1405.

Knoll, A.H., 2000. Learning to tell Neoproterozoic time. Precambrian Research 100 (1–3), 3–20.

Kronberg, B. I., Nesbitt, H. W., & Lam, W. W.,1986. Upper Pleistocene Amazon deep-sea fan muds reflect intense chemical weathering of their mountainous source lands. Chemical Geology, 54(3-4), 283-294.

Kuchenbecker, M., Babinski, M., Pedrosa-Soares, A. C., Lopes-Silva, L., & Pimenta, F., 2016. Chemostratigraphy of the lower Bambuí Group, southwestern São Francisco Craton, Brazil: insights on Gondwana paleoenvironments. Brazilian Journal of Geology, 46, 145-162.

Lehmann, B., Nägler, T. F., Holland, H. D., Wille, M., Mao, J., Pan, J., Dulski, P., 2007. Highly metalliferous carbonaceous shale and Early Cambrian seawater. Geology, 35(5), 403-406.

Karfunkel, J., Hoppe, A., 1988. Late Precambrian glaciation in central-eastern Brazil: Synthesis and model. Palaeogeography Palaeoclimatology Palaeoecology 65, 1–21.

Klinkhammer, G. P., & Palmer, M. R., 1991. Uranium in the oceans: where it goes and why. Geochimica et Cosmochimica Acta, 55(7), 1799-1806.

Kunzmann, M., Halverson, G. P., Sossi, P. A., Raub, T. D., Payne, J. L., & Kirby, J., 2013. Zn isotope evidence for immediate resumption of primary productivity after snowball Earth. Geology, 41(1), 27-30.

Kunzmann, M., Halverson, G. P., Scott, C., Minarik, W. G., & Wing, B. A., 2015. Geochemistry of Neoproterozoic black shales from Svalbard: Implications for oceanic redox conditions spanning Cryogenian glaciations. Chemical Geology, 417, 383-393.

Lawrence, M.G., Kamber, B.S., 2006. The behaviour of the rare earth elements during estuarine mixing revisited. Mar. Chem. 100, 147–161.

Lawrence, M.G., Greig, A., Collerson, K.D., Kamber, B.S., 2006. Rare earth element and yttrium variability in South East Queensland waterways. Aquat. Geochem.12, 39–72.

Li, C., Love, G. D., Lyons, T. W., Fike, D. A., Sessions, A. L., & Chu, X., 2010. A stratified redox model for the Ediacaran ocean. Science, 328(5974), 80-83.

Li, D., Ling, H. F., Shields-Zhou, G. A., Chen, X., Cremonese, L., Och, L., & Manning, C. J., 2013. Carbon and strontium isotope evolution of seawater across the Ediacaran–Cambrian transition: evidence from the Xiaotan section, NE Yunnan, South China. Precambrian Research, 225, 128-147.

Li, Y., Fan, T., Zhang, J., Zhang, J., Wei, X., Hu, X., Fu, W., 2015. Geochemical changes in the Early Cambrian interval of the Yangtze Platform, South China: Implications for hydrothermal influences and paleocean redox conditions. Journal of Asian Earth Sciences, 109, 100-123.

Li, W. P., Zheng, Y. F., & Zhao, Y. Y., 2017. Geochemical evidence from marine carbonate for enhanced terrigenous input into seawater during the Ediacaran-Cambrian transition in South China. Precambrian Research, 291, 83-97.

Lord III, C.J., 1982. A selective and precise method for pyrite determination in sedimentary materials. J. Sediment. Petrol. 52, 664– 666.

Lyons, T. W., & Severmann, S., 2006. A critical look at iron paleoredox proxies: New insights from modern euxinic marine basins. Geochimica et Cosmochimica Acta, 70(23), 5698-5722.

Ma, K., Hu, S., Wang, T., Zhang, B., Qin, S., Shi, S., & Qingyu, H., 2017. Sedimentary environments and mechanisms of organic matter enrichment in the Mesoproterozoic Hongshuizhuang Formation of northern China. Palaeogeography, Palaeoclimatology, Palaeoecology, 475, 176-187.

Mackey, T. J., Sumner, D. Y., Hawes, I., Jungblut, A. D., Lawrence, J., Leidman, S., & Allen, B., 2017. Increased mud deposition reduces stromatolite complexity. Geology, 45(7), 663-666.

Martins, M., Lemos, V.B., 2007. Análise estratigráfica das sequências neoproterozóicas da Bacia do São Francisco. Revista Brasileira de Geociências 37 (4-suplemento), 156–167.

Martins-Neto, M. A., 2009. Sequence stratigraphic framework of Proterozoic successions in eastern Brazil. Marine and Petroleum Geology, 26(2), 163-176.

Martins-Neto, M.A., Alkmim, F.F., 2001. Estratigrafia e evoluc¸ ão tectônica das bacias neoproterozóicas do paleocontinente São Francisco e suas margens: registro da quebra de Rodínia e colagem de Gondwana. In: Pinto C.P., Martins-Neto M.A. (Eds.), Bacia do São Francisco: Geologia e Recursos Naturais, SBG/MG, pp. 9–30.

Martins-Neto, M. A., Pedrosa-Soares, A. C., & Lima, S. A. D. A., 2001. Tectono-sedimentary evolution of sedimentary basins from Late Paleoproterozoic to Late Neoproterozoic in the Sao Francisco craton and Araçuaı fold belt, eastern Brazil. Sedimentary Geology, 141, 343-370.

Maruyama, S., & Santosh, M., 2008. Models on snowball Earth and Cambrian explosion: a synopsis. Gondwana Research, 14(1-2), 22-32.

McManus, J., Berelson, W. M., Klinkhammer, G. P., Hammond, D. E., & Holm, C., 2005. Authigenic uranium: relationship to oxygen penetration depth and organic carbon rain. Geochimica et Cosmochimica Acta, 69(1), 95-108.

Meert, J. G., & Lieberman, B. S., 2008. The Neoproterozoic assembly of Gondwana and its relationship to the Ediacaran–Cambrian radiation. Gondwana Research, 14(1-2), 5-21.

Miller, A. J., Strauss, J. V., Halverson, G. P., Macdonald, F. A., Johnston, D. T., & Sperling, E. A., 2017. Tracking the onset of Phanerozoic-style redox-sensitive trace metal enrichments: New results from basal Ediacaran post-glacial strata in NW Canada. Chemical Geology, 457, 24-37.

Misi, A., Iyer, S.S., Coelho, C.E.S., Tassinari, C.C.G., Franca-Rocha, W.J.S., Cunha, I.A., Gomes, A.S.R., Oliveira, T.F., Teixeira, J.B.G., Mônaco Filho, V., 2005. Sediment hosted lead–zinc deposits of the Neoproterozoic Bambuí Group and correlative sequences, São Francisco craton, Brazil: A review and a possible metallogenic evolution model. Ore Geology Reviews 26, 263–304.

Misi, A., Kaufman, A.J., Veizer, J., Powis, K., Azmy, K., Boggiani, P.C., Gaucher, C., Teixeira, J.B., Sanches, A.L., Iyer, S.S., 2007. Chemostratigraphic correlation of Neoproterozoic successions in South America. Chemical Geology 237, 143–167.

Nesbitt, H., & Young, G. M., 1982. Early Proterozoic climates and plate motions inferred from major element chemistry of lutites. Nature, 299(5885), 715.

Novo, T.A., 2009. Significado geotectônico das rochas charnockíticas da região de Carangola: implicações para a conexão Araçuaí-Ribeira. Master Thesis. Universidade Federal de Minas Gerais, Belo Horizonte, Brasil, p. 87.

Och, L. M., & Shields-Zhou, G. A., 2012. The Neoproterozoic oxygenation event: environmental perturbations and biogeochemical cycling. Earth-Science Reviews, 110(1), 26-57.

Okubo J., Muscente A.D., Luvizotto G.L., Uhlein G.J., Warren L.V. 2018. Phosphogenesis, aragonite fan formation and seafloor environments following the Marinoan glaciation. Precambrian Research, 311, 24-36.

Paula-Santos, G.M., Babinski, M., Kuchenbecker, M., Caetano-Filho, S., Trindade, R.I.F., Pedrosa-Soares, A.C., 2015. New evidence of an Ediacaran age for the Bambuí Group in southern São Francisco craton (eastern Brazil) from zircon U-Pb data and isotope chemostratigraphy. Gondwana Res. 18, 1-19.

Paula-Santos, G.M., Caetano-Filho, S., Babinski, M., Trindade, R.I., Guacaneme, C., 2017. Tracking connection and restriction of West Gondwana São Francisco Basin through isotope chemostratigraphy. Gondwana Research 42: 280-305.

Paula-Santos, G.M., Caetano-Filho, S., Babinski, M., Enzweiler, J., 2018. Rare earth elements of carbonate rocks from the Bambuí Group, southern São Francisco Basin, Brazil, and their significance as paleoenvironmental proxies. Precambrian Research 305: 327-340.

Pi, D., Liu, C., Shields-Zhou, G.A., Jiang, S., 2013. Trace and rare earth element geochemistry of black shale and kerogen in the early Cambrian Niutitang Formation in Guizhou province, South China. Precambrian Research 225, 218–229.

Pimentel, M.M., Dardenne, M.A., Fuck, R.A., Viana, M.G., Junges, S.L., Fischel, D.P., Seer, H.J., Dantas, E.L., 2001. Nd isotopes and the provenance of detrital sediments of the Neoproterozoic Brasília Belt, central Brazil. J. S. Am. Earth Sci. 14, 571-585.

Pimentel, M. M., Rodrigues, J. B., DellaGiustina, M. E. S., Junges, S., Matteini, M., & Armstrong, R., 2011. The tectonic evolution of the Neoproterozoic Brasília Belt, central Brazil, based on SHRIMP and LA-ICPMS U–Pb sedimentary provenance data: a review. Journal of South American Earth Sciences, 31(4), 345-357.

Pimentel, M. M., Della Giustina, M. E. S., Rodrigues, J. B., & Junges, S. L. (2012). Idades dos grupos Araxá e Bambuí: Implicações para a evolução da Faixa Brasília. In XLVI Congresso Brasileiro de Geologia. Santos: SBG.

Planavsky, N. J., Rouxel, O. J., Bekker, A., Lalonde, S. V., Konhauser, K. O., Reinhard, C. T., & Lyons, T. W., 2010. The evolution of the marine phosphate reservoir. Nature, 467(7319), 1088-1090.

Poulton, S. W., & Canfield, D. E., 2011. Ferruginous conditions: a dominant feature of the ocean through Earth's history. Elements, 7(2), 107-112.

Poulton, S. W., & Canfield, D. E., 2005. Development of a sequential extraction procedure for iron: implications for iron partitioning in continentally derived particulates. Chemical Geology, 214(3-4), 209-221.

Raiswell, R., & Canfield, D. E., 1998. Sources of iron for pyrite formation in marine sediments. American Journal of Science, 298(3), 219-245.

Reis, C., 2013. Geologia, Sistemas Deposicionais e Estratigrafia Isotópica do Grupo Bambuí na Região de Santa Maria da Vitória, Ba. 2013. 97f (Msc dissertation, Instituto de Geociências, Universidade de Brasília, Brasília).

Reis, H.L.S., Alkmim, F.F., 2015. Anatomy of a basin-controlled foreland fold-thrust belt curve: the Três Marias salient, São Francisco basin, Brazil. Mar. Pet. Geol.

Reis, H. L., & Suss, J. F., 2016. Mixed carbonate–siliciclastic sedimentation in forebulge grabens: An example from the Ediacaran Bambuí Group, São Francisco Basin, Brazil. *Sedimentary Geology*, *339*, 83-103.

Rocha-Campos, A.C., Hasui, Y., 1981. Tillites of the Macaúbas Group (Proterozoic) in central Minas Gerais and southern Bahia, Brazil. In: Hambrey, M.J., Harland, W.B. (Eds.), Earths's pre-Pleistocene Glacial Record. Cambridge University Press, pp. 933–939.

Rodler, A. S., Frei, R., Gaucher, C., & Germs, G. J. B., 2016. Chromium isotope, REE and redox-sensitive trace element chemostratigraphy across the late Neoproterozoic Ghaub glaciation, Otavi Group, Namibia. Precambrian Research, 286, 234-249.

Roser, B. P., & Korsch, R. J. (1988). Provenance signatures of sandstone-mudstone suites determined using discriminant function analysis of major-element data. Chemical geology, 67(1-2), 119-139.

Sahoo, S. K., Planavsky, N. J., Kendall, B., Wang, X., Shi, X., Scott, C., & Jiang, G., 2012. Ocean oxygenation in the wake of the Marinoan glaciation. Nature, 489(7417), 546-549.

Sampaio, G. M. S., & Enzweiler, J., 2015. New ICP-MS Results for Trace Elements in Five Iron-Formation Reference Materials. Geostandards and Geoanalytical Research, 39(1), 105-119.

Santos, R.V., Alvarenga, C.J.S., Dardenne, M.A., Sial, A.N., Ferreira, V.P., 2000. Carbon and oxygen isotope profiles across Meso-Neoproterozoic limestones from central Brazil: Bambuí and Paranoá groups. Precambrian Research 104, 107–122.

Scott, C., Lyons, T. W., Bekker, A., Shen, Y. A., Poulton, S. W., Chu, X. L., & Anbar, A. D., 2008. Tracing the stepwise oxygenation of the Proterozoic ocean. *Nature*, *452*(7186), 456-459.

Scott, C., & Lyons, T. W., 2012. Contrasting molybdenum cycling and isotopic properties in euxinic versus non-euxinic sediments and sedimentary rocks: Refining the paleoproxies. Chemical Geology, 324, 19-27.

Shen, B., Xiao, S., Zhou, C., Kaufman, A. J., & Yuan, X., 2010. Carbon and sulfur isotope chemostratigraphy of the Neoproterozoic Quanji Group of the Chaidam Basin, NW China: Basin stratification in the aftermath of an Ediacaran glaciation postdating the Shuram event?. Precambrian Research, 177(3), 241-252.

Schröder, S., & Grotzinger, J. P., 2007. Evidence for anoxia at the Ediacaran–Cambrian boundary: the record of redox-sensitive trace elements and rare earth elements in Oman. Journal of the Geological Society, 164(1), 175-187.

Shields, G., & Stille, P., 2001. Diagenetic constraints on the use of cerium anomalies as palaeoseawater redox proxies: an isotopic and REE study of Cambrian phosphorites. Chemical Geology, 175(1), 29-48.

Spangenberg, J. E., Bagnoud-Velásquez, M., Boggiani, P. C., & Gaucher, C., 2014. Redox variations and bioproductivity in the Ediacaran: Evidence from inorganic and organic geochemistry of the Corumbá Group, Brazil. Gondwana Research, 26(3), 1186-1207.

Sperling, E. A., Halverson, G. P., Knoll, A. H., Macdonald, F. A., & Johnston, D. T., 2013. A basin redox transect at the dawn of animal life. Earth and Planetary Science Letters, 371, 143-155.

Sweere, T., van den Boorn, S., Dickson, A. J., & Reichart, G. J., 2016. Definition of new trace-metal proxies for the controls on organic matter enrichment in marine sediments based on Mn, Co, Mo and Cd concentrations. Chemical Geology, 441, 235-245.

Taylor, S. R., & McLennan, S. M., 1985. The continental crust: its composition and evolution.

Tribovillard, N., Algeo, T. J., Lyons, T., & Riboulleau, A., 2006. Trace metals as paleoredox and paleoproductivity proxies: an update. Chemical geology, 232(1), 12-32.

Turekian, K. K., & Wedepohl, K. H., 1961. Distribution of the elements in some major units of the earth's crust. Geological Society of America Bulletin, 72(2), 175-192.

Uhlein, A., Alvarenga, C.J.S., Dardenne, M.A., Trompette, R.R. 2011. The glaciogenic Jequitaí Formation, southeastern Brazil. In: E. Arnaud, G. P. Halverson and G. Shields-Zhou (Eds.) The Geological Record of Neoproterozoic Glaciations. Geological Society of London, London, Memoir vol. 36, 51–66.

Uhlein, G.J., Carvalho, J.F.M.G., Uhlein, A., Caxito, F.A., Halverson, G.P., Sial, A., 2012. Estratigrafia e Sedimentologia da Formação Carrancas, Grupo Bambuí, nas regiões de Belo Horizonte e Pitangui. MG. Geonomos 20 (2), 79–97.

Uhlein, G. J., Uhlein, A., Halverson, G. P., Stevenson, R., Caxito, F. A., Cox, G. M., & Carvalho, J. F., 2016. The Carrancas Formation, Bambuí Group: A record of pre-Marinoan sedimentation on the southern São Francisco craton, Brazil. Journal of South American Earth Sciences, 71, 1-16.

Uhlein, G.J., Uhlein, A., Stevenson, R., Halverson, G.P., Caxito, F.A., Cox, G.M., 2017. Early to late Ediacaran conglomeratic wedges from a complete foreland basin cycle in the southwest São Francisco Craton, Bambuí Group, Brazil. Precambrian Research 299, 101–116.

Van der Weijden, C. H., 2002. Pitfalls of normalization of marine geochemical data using a common divisor. Marine Geology, 184(3), 167-187.

Vieira, L.C. A Formação Sete Lagoas (Grupo Bambuí) e as variações paleoambientais no final do Proterozóico. 2007. 190 pp. Phd thesis – Instituto de Astronomia, Geofísica e Ciências Atmosféricas, Universidade de São Paulo, São Paulo, 2007.

Vieira, L.C., Trindade, R.I.F., Nogueira, A.C.R., Ader, M., 2007. Identification of a Sturtian cap carbonate in the Neoproterozoic Sete Lagoas carbonate platform, Bambuí Group, Brazil. Comptes Rendus Geoscience 339, 240–258.

Vieira, V.S., 2007. Significado do Grupo Rio Doce no Contexto do Or_ogeno Araçuaí. Ph.D. thesis. Universidade Federal de Minas Gerais, Belo Horizonte, Brazil, p. 117.

Zhai, L., Wu, C., Ye, Y., Zhang, S., & Wang, Y., 2018. Fluctuations in chemical weathering on the Yangtze Block during the Ediacaran–Cambrian transition: Implications for paleoclimatic conditions and the marine carbon cycle. Palaeogeography, Palaeoclimatology, Palaeoecology, 490, 280-292.

Wallace, M. W., Shuster, A., Greig, A., Planavsky, N. J., & Reed, C. P., 2017. Oxygenation history of the Neoproterozoic to early Phanerozoic and the rise of land plants. Earth and Planetary Science Letters, 466, 12-19.

Wanty, R. B., & Goldhaber, M. B., 1992. Thermodynamics and kinetics of reactions involving vanadium in natural systems: Accumulation of vanadium in sedimentary rocks. Geochimica et Cosmochimica Acta, 56(4), 1471-1483.

Warren, L.V., Quaglio, F., Riccomini, C., Simoes, M.G., Poire, D.G., Strikis, N.M., Anelli, L.E., Strikis, P.C., 2014. The puzzle assembled: Ediacaran guide fossil Cloudina reveals an old proto-Gondwana seaway. Geology 42, 391-394.

Webb, G. E., Nothdurft, L. D., Kamber, B. S., Kloprogge, J. T., & ZHAO, J. X., 2009. Rare earth element geochemistry of scleractinian coral skeleton during meteoric diagenesis: a sequence through neomorphism of aragonite to calcite. Sedimentology, 56(5), 1433-1463.